

Article

# Study on the Curing and Foaming of Surfactant-Modified Geopolymer Gels Based on Ash and Slag Waste from Coal Combustion

Elena A. Yatsenko <sup>1</sup>, Sergei V. Trofimov <sup>1,\*</sup>, Boris M. Goltsman <sup>1</sup>, Wensheng Li <sup>2</sup>, Victoria A. Smoliy <sup>1</sup>, Anna V. Ryabova <sup>1</sup>, Lyudmila V. Klimova <sup>1</sup> and Andrey I. Izvarin <sup>1</sup>

- <sup>1</sup> Department “General Chemistry and Technology Silicates”, Platov South-Russian State Polytechnic University (NPI), Prosveshcheniya Street 132, Rostov Region, 346428 Novocherkassk, Russia; e\_yatsenko@mail.ru (E.A.Y.); b.goltsman@npi-tu.ru (B.M.G.); vikk-toria@yandex.ru (V.A.S.); annet20002006@yandex.ru (A.V.R.); lyudmila.clim@yandex.ru (L.V.K.); andre.izvarin@yandex.ru (A.I.I.)
- <sup>2</sup> College of Physics and Electronic Engineering, Northwest Normal University, Lanzhou 730070, China; liws@nwnu.edu.cn
- \* Correspondence: 23zarj23@mail.ru

**Abstract:** This study explores the influence of temperature–time conditions, surfactants, and varied waste compositions on the curing of geopolymer gels, a foam formation with the properties of porous geopolymers. Findings reveal that a 6 h curing period leads to a density of 435 kg/m<sup>3</sup> and strength of 0.66 MPa, with notable improvements at 12 h. Comparing 12 to 24 h curing, differences in characteristics remain within 5%, highlighting the 12 h period as more energy-efficient. Sodium stearate-based samples exhibit excellent properties, significantly boosting strength while maintaining overall properties. Microwave curing achieves the lowest density (291 kg/m<sup>3</sup>) and closely parallels properties of samples cured conventionally for 12 h. However, it leads to complete destruction in sodium stearate-modified gels due to the Dumas reaction, making it unsuitable above 200 °C. Optimal properties emerge from compositions using sodium stearate and oven curing, achieving densities of 334 kg/m<sup>3</sup> and strengths of 1.08 MPa (Severodvinsk CHPP-1) and 373 kg/m<sup>3</sup> and 1.17 MPa (Novocherkassk SDPP). Although microwave curing allows for high energy efficiency, its high temperature demands necessitate careful material selection. This study offers insight into enhancing geopolymer properties while emphasizing the importance of tailored curing methods for sustainable material development.

**Keywords:** geopolymer; ash and slag waste; porous structure; surfactant; sodium stearate; microwave curing; the Dumas reaction



**Citation:** Yatsenko, E.A.; Trofimov, S.V.; Goltsman, B.M.; Li, W.; Smoliy, V.A.; Ryabova, A.V.; Klimova, L.V.; Izvarin, A.I. Study on the Curing and Foaming of Surfactant-Modified Geopolymer Gels Based on Ash and Slag Waste from Coal Combustion. *Gels* **2024**, *10*, 19. <https://doi.org/10.3390/gels10010019>

Academic Editor: Mario Grassi

Received: 18 November 2023

Revised: 14 December 2023

Accepted: 21 December 2023

Published: 23 December 2023



**Copyright:** © 2023 by the authors. Licensee MDPI, Basel, Switzerland. This article is an open access article distributed under the terms and conditions of the Creative Commons Attribution (CC BY) license (<https://creativecommons.org/licenses/by/4.0/>).

## 1. Introduction

Currently, environmentally friendly geopolymer materials are gaining increasing popularity worldwide due to their promising combination of physical–chemical properties and low production costs, which is confirmed by a large number of review articles [1–5]. According to J. Davidovits, geopolymers are inorganic materials obtained by alkaline (less frequently acidic [6]) activation of aluminosilicate components present in natural, artificial, or industrial raw materials. The detailed mechanism of geopolymer formation (the geopolymerization reaction) was presented by Rao et al. and Lemoungna et al. [7,8].

Depending on the area of application and the required properties, a distinction is made between porous geopolymer materials (geopolymer foam) and geopolymer concrete. Porous geopolymer materials have such promising properties as high porosity (more than 80%) associated with low density (0.30–0.80 g/cm<sup>3</sup>), thermal conductivity (0.05–0.11 W/(m·K)), and compressive strength (0.2–5.47 MPa) [9–12]. The potential use

of porous geopolymer materials is possible in a fairly wide range, for example, as sorbents for purifying wastewater from chemical and biological pollutants or heavy metals [1,4,13,14], materials for fire protection of construction [2,15,16], catalysts for the synthesis of biodiesel [17,18], as well as in the form of multifunctional coatings for both thermal [7,19] and acoustic insulation [20,21].

Various aluminosilicate raw materials are used for synthesizing geopolymers: natural raw materials include kaolin, volcanic ash, etc. [22,23]; artificial raw materials include metakaolin, metagalluazite, etc. [10,24,25]; and various industrial waste materials include solid fuel residues (ashes, slag, and ash–slag mixtures), rice husk ash, etc. [26–30]. However, it is preferable to use raw materials with a high content of an amorphous phase due to improved reactivity [31]. Utilizing waste as aluminosilicate raw material is more advantageous as it reduces environmental impact while enhancing the economic efficiency of geopolymer production by utilizing easily accessible materials. The most large-capacity among them is ash and slag waste (ASW). According to various estimates, from 750 to 900 million tons of ASW is generated annually around the world [32,33].

The porosity strongly influences the physical and mechanical properties of porous geopolymer materials [2,3,34,35]. Porosity depends on various factors: the type and concentration of foaming and stabilizing additives, as well as the temperature–time curing mode [5]. The most common and easily accessible foaming agents are hydrogen peroxide ( $H_2O_2$ ) with concentrations ranging from 3 to 35% [36,37], and metal powders [38]. Other agents are also utilized: for example, aluminum powder (Al) [39], silicon carbide (SiC) [40], microsilica [41], sodium perborate ( $NaBO_3$ ) [42], etc. Foam stabilizers (surfactants) also influence the porosity of the geopolymer and its physical and mechanical properties [35,43]. Different substances are employed as surfactants: palm and sunflower oils [44,45], calcium or sodium stearates [45,46], sodium dodecyl sulfate [47], and others. In review publications [21,35,48], the most common chemical surfactants are calcium stearate and sodium dodecyl sulfate, as they reduce the maximum pore size to 2 mm and improve pore distribution, thereby enhancing the mechanical properties of geopolymers. Among vegetable oils, studies have been conducted with sunflower, palm, olive, and canola oil. Their introduction also allows reducing surface tension. However, the obtained structures are not sufficiently stable and lead to the formation of interconnected pores, distinguishing oils from chemical and commercial surfactants.

Regarding the temperature–time curing modes, low-temperature (20–120 °C [49,50]) and high-temperature treatments (firing) at temperatures of 600–1000 °C [51] are applied. High temperatures positively impact the mechanical properties of products while simultaneously increasing density, thermal conductivity, and energy consumption [52]. Low-temperature curing is more commonly used as it leads to more stable foam formation, positively influencing porosity and density [50].

Microwave curing is less common. Microwaves have the ability to penetrate almost any material and release energy within, heating the entire volume rapidly. Theoretically, this simplifies process control and reduces the cost of synthesizing various materials. Microwaves can be particularly useful for manufacturing porous geopolymers since these materials exhibit low thermal conductivity, and microwave radiation can significantly enhance heat transfer throughout the material. In a series of studies [53–56], microwave curing was utilized to obtain porous geopolymers without the use of a foaming agent—the foaming occurred due to water evaporation during rapid material heating. Different concentrations of alkali activators from 2 to 15 M (NaOH, KOH) were employed in the investigations, showing improved density results (from 5000 kg/m<sup>3</sup> to 330 kg/m<sup>3</sup>) with increased concentration. It is noteworthy that in study [54], after microwave curing, they subjected empty coal rock to firing within the temperature range of 500–1100 °C, which does not render the technology energy-efficient. In the study [57], there was also no foaming agent used. However, soybean oil was employed for emulsification and microwave foaming. This method allowed for obtaining porous geopolymers with outstanding results: a density of 287 kg/m<sup>3</sup> and a strength of 0.45 MPa. These studies confirm that microwave

radiation is an innovative method for accelerated heating and, consequently, intensifying the chemical reaction rates.

In the final analysis of articles on microwave curing, no studies were found that examined the combined influence of surfactants of plant and chemical origin with microwave curing. Based on this, the authors set the task of studying the combined effect of microwave curing and surfactants on the formation of the structure and physical–chemical properties of porous geopolymers. This study aims to contribute to the exploration of porous geopolymers as a promising material and in the future, assist in being more attentive to the selection of raw materials and curing mode for synthesizing porous geopolymers.

## 2. Results and Discussion

### 2.1. Optimization of Temperature–Time Mode in the Drying Oven

Preliminarily, the authors investigated curing modes in a drying oven at temperatures of 60, 70, 80, and 90 °C with a duration of 24 h. The optimal mode was found to be at a temperature of 80 °C. It is considered that as the curing time increases, there is an improvement in the ultimate compressive strength of the samples, as the geopolymerization reaction occurs within 20–24 h [58]. However, this mode cannot be considered energy-efficient since the drying oven (at  $P = 1200$  W) consumes approximately 5800 W of electricity over 24 h. Therefore, there was a decision to assess the possibility of optimizing the curing time to reduce energy consumption while maintaining the physical–chemical properties at the same level.

To address this task, the mass loss of the samples was measured over 24 h with a 30 min interval to identify the constant mass point. The mass is considered constant if three consecutive measurements differ by no more than 0.1 mass%. The mass loss is presented in Figure 1a. The investigation of the physical–chemical characteristics (density, ultimate compressive strength) of the samples was conducted every 6 h during curing. The obtained data are depicted in Figure 1b.

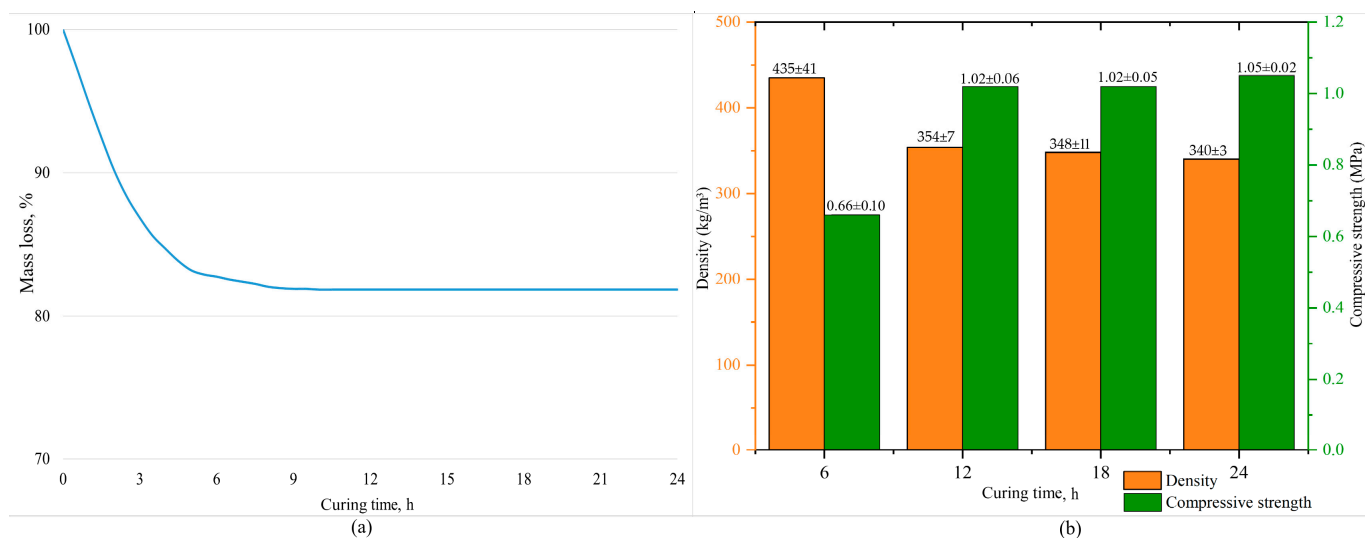


**Figure 1.** Mass loss (a) and physical–chemical properties of porous geopolymers (b).

The Figure shows that the samples with the maximum curing time have the lowest density ( $340 \pm 3$  kg/m<sup>3</sup>) and the highest strength ( $1.05 \pm 0.02$  MPa). After 6 h of start of curing, demolded samples were partially destructed. The physical and mechanical characteristics of these samples are at an extremely low level: the compressive strength accounts for 60% of the maximum value, and the density exceeds the minimum by 28%, which is an unsatisfactory result. This is due to the fact that this curing duration is insufficient for the geopolymerization reaction to complete at 80 °C. However, accelerating the process by increasing the temperature could increase the pore volume or lead to the

formation of cracks in the geopolymer material, negatively impacting the compressive strength of the samples. This result is in accordance with other studies [59].

Extending the curing time from 6 to 12 h increases the density and strength by an average of 23% and 55%, respectively. With further extension from 12 to 18 h, a slight decrease in density and an average increase in strength of 2% were observed. This trend persisted with the maximum curing time. Ultimately, the difference between 12 and 24 h of curing is no more than 5%, highlighting the 12 h as the most optimal choice for curing time.

## 2.2. Physical–Mechanical Properties of Synthesized Porous Geopolymers

The internal structure and physical–mechanical properties of the synthesized samples presented in Figure 2 and Table 1. Figure 3 shows pore size distribution in the samples. The ranges of pore distribution for different compositions are presented in Table 2.

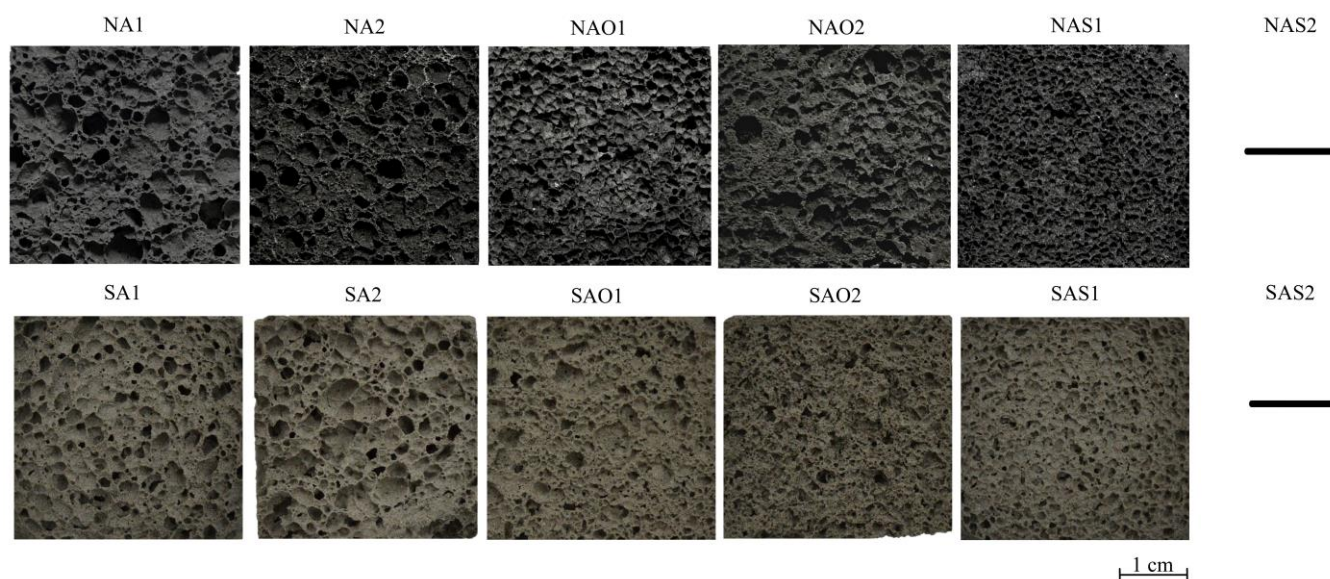


Figure 2. Internal structure of the synthesized porous geopolymers.

Table 1. Medium physical–mechanical properties of the synthesized porous geopolymers.

#	Density, kg/m <sup>3</sup>	Compressive Strength, MPa	Porosity, %	Thermal Conductivity, W/(m·K)
NA1	339 ± 11	0.88 ± 0.05	85.8 ± 0.2	0.0754 ± 0.0038
NA2	322 ± 15	0.83 ± 0.03	87.7 ± 0.7	0.0719 ± 0.0031
NAO1	364 ± 14	0.86 ± 0.02	84.8 ± 0.8	0.0750 ± 0.0031
NAO2	361 ± 18	0.77 ± 0.06	84.9 ± 0.9	0.0800 ± 0.0009
NAS1	373 ± 7	1.17 ± 0.08	84.3 ± 1.0	0.0826 ± 0.0018
SA1	306 ± 3	0.85 ± 0.03	85.0 ± 0.1	0.0700 ± 0.0005
SA2	291 ± 5	0.83 ± 0.03	85.7 ± 0.7	0.0670 ± 0.0008
SAO1	326 ± 4	0.78 ± 0.03	84.0 ± 0.2	0.0745 ± 0.0009
SAO2	322 ± 9	0.73 ± 0.02	84.1 ± 0.9	0.0736 ± 0.0014
SAS1	334 ± 11	1.08 ± 0.03	83.6 ± 0.6	0.0761 ± 0.0021

The absence of a structure for the NAS2 and SAS2 compositions in Figure 2 is explained by the complete destruction of these samples. The result is presented on Figure 4a.

This occurs only with compositions using sodium stearate and microwave curing. After exposure to microwave radiation, the geopolymer was a granular material in the form of cemented particles. Using a thermal imager, it was observed that the outer part of the sample heated to 220 °C (Figure 4b). Simultaneously, the central part heated to 608 °C, a critical point for this composition. A detailed examination of this result is presented in Section 2.4.

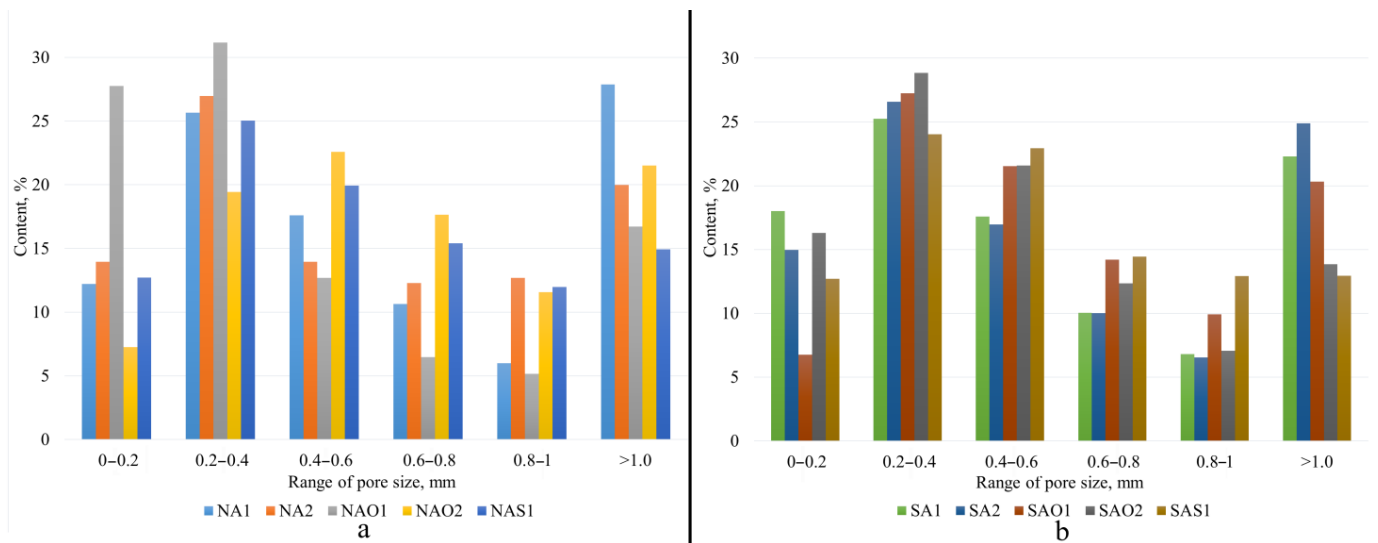


Figure 3. Pore size distribution ranges: (a)—Novochoerkassk SDPP, (b)—Severodvinsk CHPP-1.

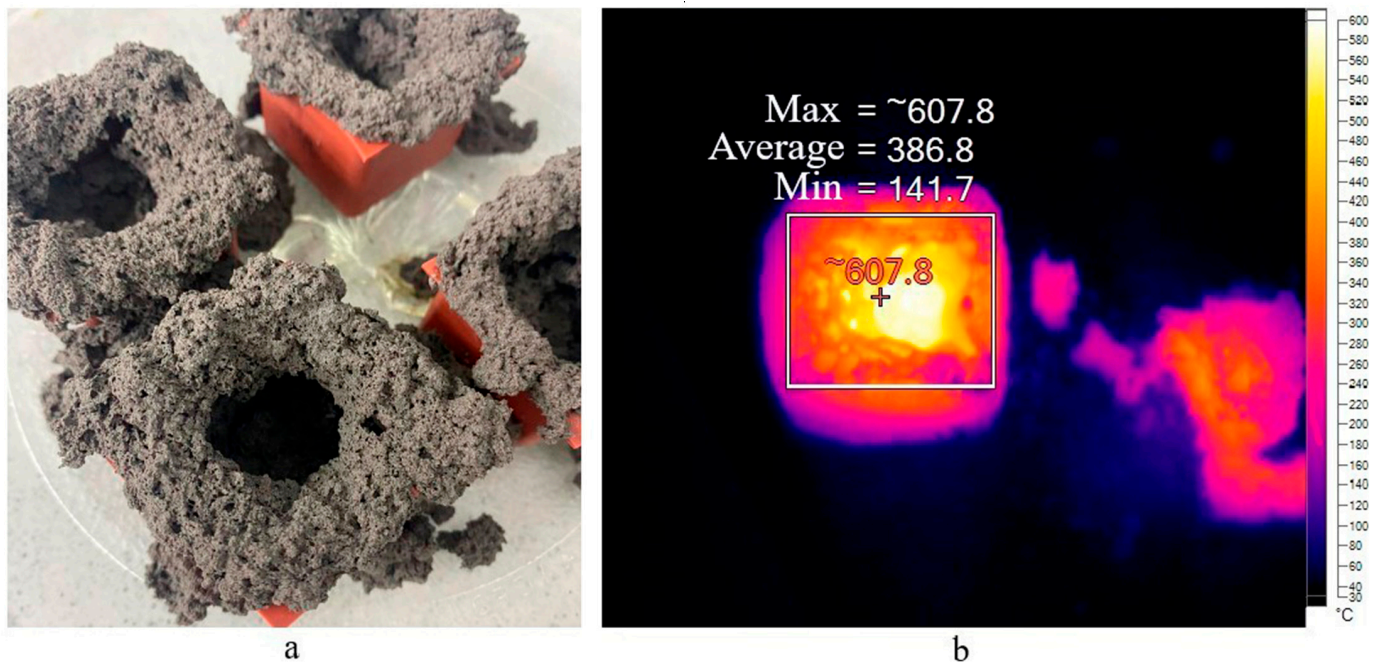


Figure 4. Appearance of destroyed samples (a) and thermal image of the sample exposed to microwave radiation (b).

According to Figure 2 and Table 1, the use of ASW with different chemical and phase compositions significantly affects the properties of porous geopolymers. Geopolymers based on ASW from Novochoerkassk SDPP have, on average, a 12% higher bulk density compared to geopolymers based on ASW from Severodvinsk CHPP-1. One of the influencing factors is the true density of ASW: ASW from Novochoerkassk SDPP has a higher true density ( $2321 \text{ kg/m}^3$ ) than ASW from Severodvinsk CHPP-1 ( $2034 \text{ kg/m}^3$ ). However, the difference in the ultimate compressive strength between the wastes is not more than 1.5%.

The curing mode has a lesser impact on the physical–mechanical properties of geopolymers compared to the type of stabilizing additive. Compositions without stabilizing agents (NA1, NA2, SA1, SA2) hereinafter will be described as base compositions. Analyzing compositions NA1 and NA2, it is evident that microwave curing demonstrates better results. Density and strength reduction are at 5% and 6%, respectively. Compositions using olive oil show a similar trend. The strength reduction using microwave radiation was 11%

at the same density. This strength reduction is linked to the morphology of foam formation, specifically with pore distribution: composition NAO2 has 50% larger pores (0.38 vs. 0.66 mm). In this study, it was found that unlike the drying oven, microwave curing has a higher material heating temperature, which adversely affected the structure formation with sodium stearate. Additionally, olive oil has a boiling point of 299 °C, increasing the intensity of chaotic foam formation. Therefore, composition NAO2 exhibits numerous large and interconnected pores, close to an oval shape. Ultimately, the combination of these factors deteriorates the strength properties of the composition. Composition NAS1 has enhanced physical–mechanical properties: with a 13% increase in density, the strength increased by 36% compared to the base compositions.

**Table 2.** The pore distribution of the synthesized porous geopolymers.

#	D50	D90	D99
NA1	0.53 ± 0.07	1.97 ± 0.03	4.24 ± 0.21
NA2	0.56 ± 0.08	1.69 ± 0.07	3.94 ± 0.17
NAO1	0.38 ± 0.03	1.48 ± 0.03	3.61 ± 0.24
NAO2	0.66 ± 0.05	1.59 ± 0.05	2.87 ± 0.18
NAS1	0.48 ± 0.04	1.34 ± 0.05	2.49 ± 0.13
SA1	0.43 ± 0.04	1.67 ± 0.06	3.53 ± 0.17
SA2	0.52 ± 0.07	1.90 ± 0.11	4.95 ± 0.21
SAO1	0.55 ± 0.05	1.17 ± 0.06	2.05 ± 0.22
SAO2	0.48 ± 0.04	1.22 ± 0.05	2.60 ± 0.22
SAS1	0.51 ± 0.04	1.34 ± 0.03	2.59 ± 0.11

The compositions based on ASW from Severodvinsk CHPP-1 demonstrate a similar trend but with better results. Compositions SA1 and SA2 have the lowest density due to randomly distributed macropores. Compositions using olive oil show a 7% higher density compared to compositions without surfactants. The use of sodium stearate also increased the physical–mechanical properties relative to the base compositions: density and strength increased by 12% and 28%, respectively.

In terms of using surfactants of different origins, sodium stearate appears to be the most optimal. A 3% increase in bulk density correlates with a 42% enhancement in sample strength compared to compositions based on olive oil.

In general, highly porous material obtained without firing technology always exhibits reduced mechanical properties while maintaining other properties. For instance, in the synthesis of porous geopolymers with acoustic insulation properties, C. Leiva et al. [60] utilized F class fly ash (FA) with the addition of paval waste containing a high content of aluminum oxide (over 75%), using KOH as an alkali, and no foaming agent was applied. Mixing them in various ratios and curing at 70 °C for 24 h resulted in geopolymers with densities ranging from 916 to 1640 kg/m<sup>3</sup> and strengths from 3.07 to 14.8 MPa. Jiahuan Shao et al. [61] employed bauxite, metakaolin, FA, and NaOH as primary materials, with hydrogen peroxide H<sub>2</sub>O<sub>2</sub> as a foaming agent. After curing in a closed plastic mold in a drying oven at 35 °C and 75 °C for a total of 48 h, the samples underwent firing at a gradual temperature increase up to 1500 °C for 3 h. Ultimately, porous geopolymers were obtained with densities from 500 to 930 kg/m<sup>3</sup>, strengths from 0.58 to 2.31 MPa, and porosities from 81 to 84%. In the study by Fang Xu et al. [47], similar raw materials (FA, NaOH, H<sub>2</sub>O<sub>2</sub>) were used, varying the initial curing temperature from 25 to 130 °C for 3 h, followed by a 28-day curing period at room temperature. The resulting geopolymers had densities from 500 to 1040 kg/m<sup>3</sup> and strengths ranging from 3.2 to 44.81 MPa. In the research of Zehua Ji et al. [62], authors used solid wastes (granulated ground blast furnace slag), drinking water treatment residual, and NaOH as primary materials, with H<sub>2</sub>O<sub>2</sub> as a foaming agent and with surfactants (sodium dodecyl sulfate, sodium alcohol ether sulfate, and disodium laureth sulfosuccinate). Curing in a drying oven at 70 °C for 24 h followed by 7 days at room temperature revealed that sodium dodecyl sulfate was the most effective

surfactant. The resulting densities were from 520 to 1330 kg/m<sup>3</sup>, strengths were from 1.76 to 12.14 MPa, and porosities were from 9.94 to 67.89%. In the research by Ehsan Ul Haq et al. [56], fly ash and NaOH (14 mol/L) were used, and the curing of porous geopolymers was conducted using 900 W microwave irradiation for 4 min. Through this study, the authors obtained specimens with densities ranging from 610 to 1300 kg/m<sup>3</sup>, strengths from 3.0 to 6.2 MPa, and porosities from 41 to 72%. The foaming of the geopolymer occurred due to the increased intensity of water evaporation.

The mechanical properties obtained in this study (Table 1) appear to fall within the same range as those reported for porous geopolymers described earlier, and even surpass them in the density values. It is also evident that utilizing a single type of raw material, such as fly ash, does not ensure the stability of physical–mechanical properties due to variations in the chemical composition of the raw material. One of the advantages of this research is the utilization of the most abundant raw materials: ASW generated from solid fuel combustion.

Figure 5 shows the mapping results of the surface of geopolymer compositions NA1 and SA1 obtained during EDAX analysis. Images of all synthesized compositions are available in Supplementary Files (Figure S1). The atomic content of elements in all compositions are presented in Table 3.

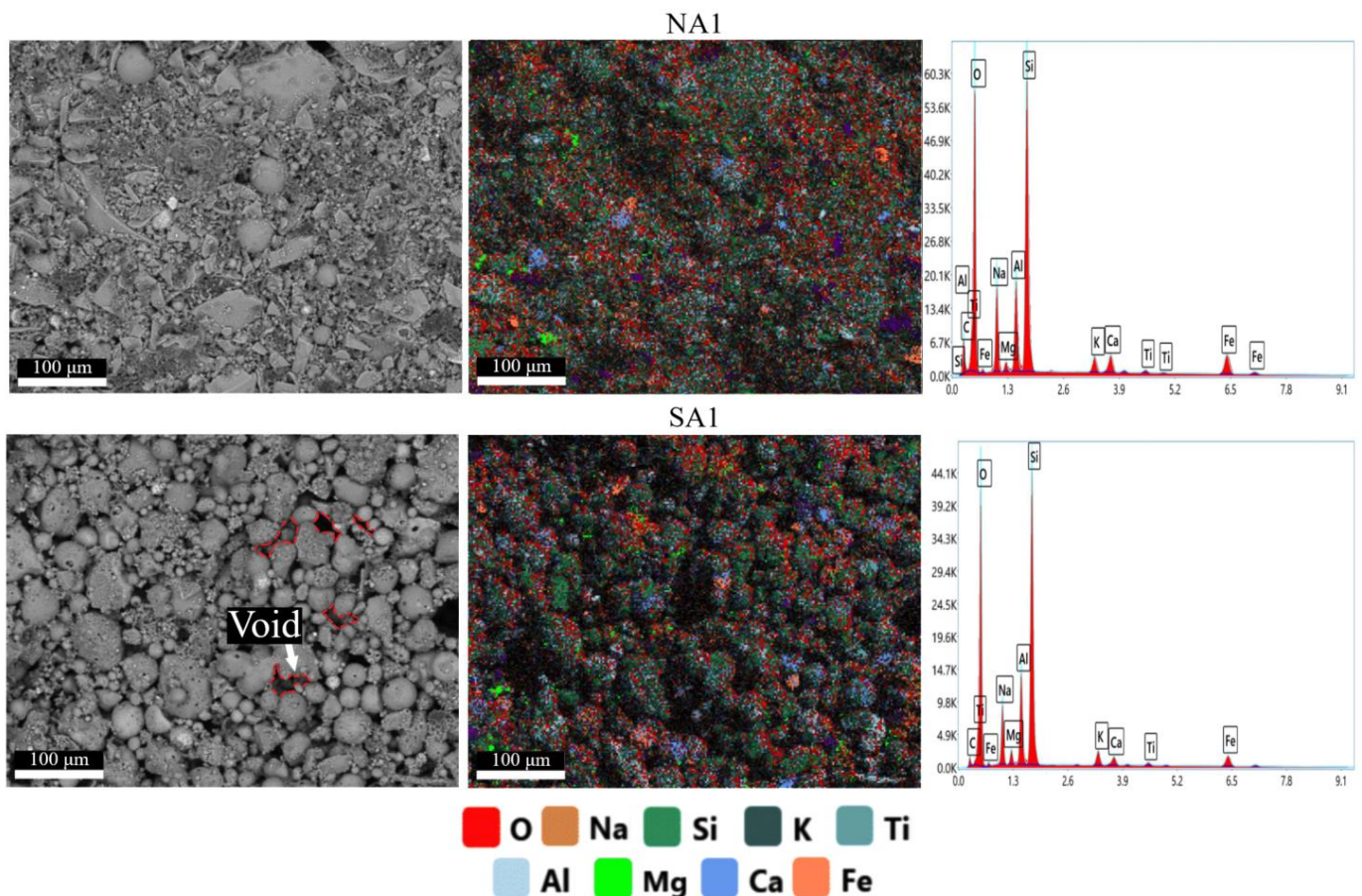


**Figure 5.** Results of elemental analysis of the surface of porous geopolymers.

These results support theoretical calculations of the developed compositions (Section 4.1, Table 5). In addition to light elements such oxygen, the most common elements found in the synthesized geopolymers are silicon, aluminum, and sodium. The use of sodium stearate leads to an increase in sodium content.

**Table 3.** Content of elements in the synthesized samples, atomic%.

Composition	O	Na	Al	Mg	Si	K	Ca	Ti	Fe	Σ
NA1	59.9	11.2	5.8	0.9	16.5	1.0	1.3	0.2	3.2	100.0
NA2	57.1	12.3	6.1	1.1	18.3	1.2	1.4	0.3	2.2	100.0
NAO1	58.3	13.7	5.6	1.0	16.7	1.1	1.4	–	2.2	100.0
NAO2	60.4	12.8	5.2	1.0	16.1	1.0	1.2	0.2	2.1	100.0
NAS1	57.1	16.7	5.1	0.9	15.9	1.0	1.2	0.2	1.9	100.0
SA1	62.1	8.4	6.2	1.4	18.3	1.0	0.8	0.3	1.5	100.0
SA2	62.4	10.9	5.6	1.3	16.9	0.9	0.6	0.2	1.2	100.0
SAO1	62.2	9.1	5.9	1.4	17.5	1.0	0.9	0.2	1.8	100.0
SAO2	62.0	9.2	6.1	1.4	17.9	1.0	0.7	0.3	1.4	100.0
SAS1	62.0	13.7	4.9	1.4	15.5	0.7	0.6	0.2	1.0	100.0

Analysis of the obtained SEM images reveals a clear distinction among particles involved in the structure formation of geopolymers. In the NA and NAS compositions, the structure is a conglomerate-type, predominantly composed of angular particles with small agglomerates of rounded particles (close to spherical). These compositions also exhibit a more continuous and dense gel phase with cemented particles, which positively influences the strength of the geopolymer. Conversely, in the SA-SAS compositions, the structure is predominantly represented by spherical or near-spherical particles. Despite a sufficient amount of amorphous gel, these spherical particles have a more porous structure with more voids between them. Their presence reduces the compressive strength and density of the synthesized geopolymers.

The obtained results demonstrate that, besides chemical composition, structure also influences the strength of synthesized geopolymers that is supported by research conducted by other authors [63].

### 2.3. XRD Analysis of Porous Geopolymers

The chosen compositions for the structural analysis were the base compositions: SA1, SA2, NA1, and NA2. This decision was made because the X-ray diffractometer only identifies the inorganic component of the material under investigation. Therefore, X-ray diffraction patterns with the application of surfactants would not differ from the base ones. Based on this, Figure 6 presents the results of X-ray phase analysis of porous geopolymers without surfactants. The content of the crystalline and amorphous phase in synthesized porous geopolymers is in Table 4.

**Table 4.** Content of crystalline and amorphous phase in synthesized porous geopolymers, wt.%.

	Low Quartz	Mullite	Hematite	Amorphous Phase
NA1	13.6 ± 0.5	–	8.0 ± 0.1	78.4 ± 0.6
NA2	15.6 ± 0.5	–	–	84.4 ± 0.4
SA1	31.3 ± 0.4	8.8 ± 0.1	–	59.9 ± 0.6
SA2	29.1 ± 0.6	7.0 ± 0.1	–	63.9 ± 0.2

All compositions contain both amorphous phase and crystalline phase in the form of quartz, mullite, and hematite. Compositions SA1 and SA2 are almost identical in terms of the crystalline phases appearance and the placement of the amorphous halo in the range of 18–34°. Composition SA1 and SA2 are represented by 59.9 ± 0.6 and 63.9 ± 0.2% of aluminosilicate amorphous phase, and 40.1 ± 0.5 and 36.1 ± 0.7% crystalline phase, respectively. The microwave exposure in composition SA2 increased the content of the amorphous phase by 4%, compared to the previous composition. This result can be explained by the positive impact of temperature on the reaction rate, especially in enhancing the dissolution of the crystalline phase by alkali.

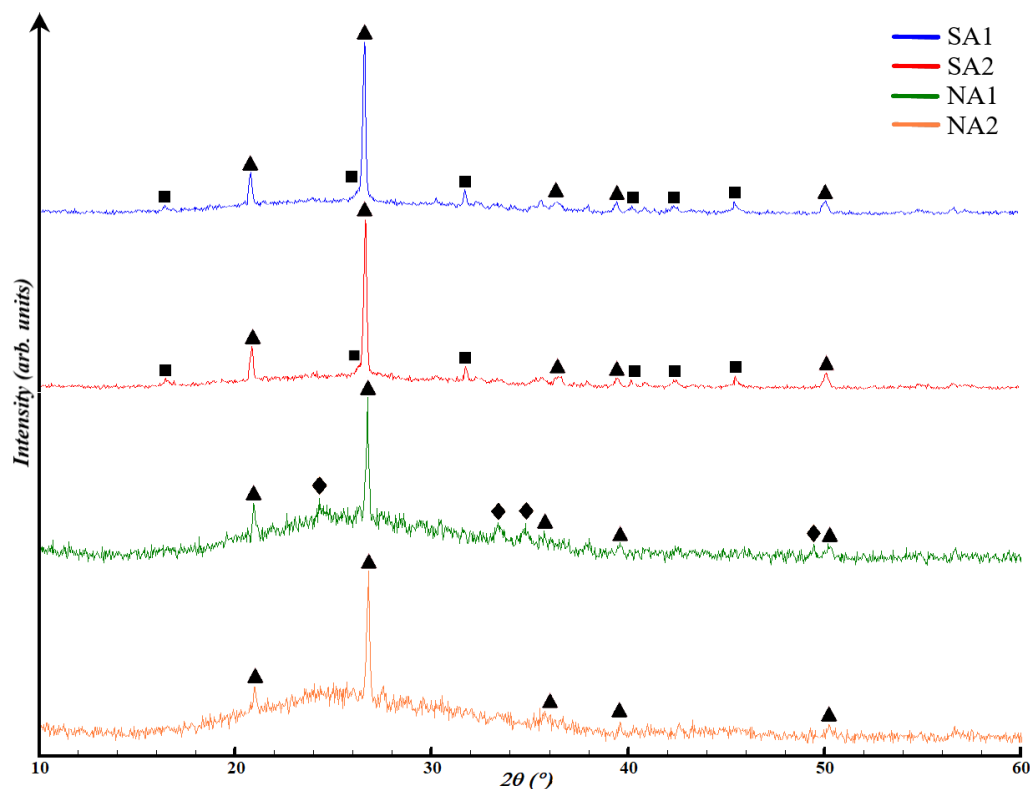
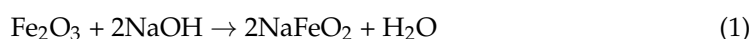


**Figure 6.** XRD curves of synthesized porous geopolymers:  $\Delta$ —low quartz ( $\text{SiO}_2$ ),  $\square$ —mullite ( $3\text{Al}_2\text{O}_3 \cdot 2\text{SiO}_2$ ),  $\diamond$ —hematite ( $\text{Fe}_2\text{O}_3$ ).

In compositions NA1 and NA2, the amorphous phase is located in the range of  $16\text{--}38^\circ$ . Composition NA1 comprises  $78.4 \pm 0.6\%$  ferroaluminosilicate amorphous phase and  $21.6 \pm 0.6\%$  crystalline phase. Composition NA2 consists of  $84.4 \pm 0.4\%$  ferroaluminosilicate amorphous phase and  $15.6 \pm 0.5\%$  crystalline phase in the form of low quartz. The increase in the amorphous phase content by 14% also occurs due to the influence of high temperature. The reduction of hematite phase can be explained by its interaction with NaOH, according to Equation (1):



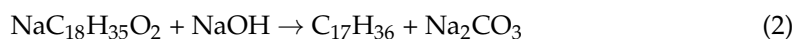
Iron (III) oxide is an amphoteric oxide, which, upon interaction with alkali during heating, forms sodium ferrate (III) with the release of water. A necessary condition for the reaction 1 to occur is heating to a temperature of at least  $600^\circ\text{C}$ . This temperature arises under the influence of microwave radiation with a power of 700 W within the time interval of 120–180 s, confirmed by thermal images of the samples described below (Section 2.4, Figure 10b).

As mentioned below in Section 4.1, ASW is represented by more than 55% amorphous phase. The results obtained show that sodium hydroxide in a 12 M solution partially dissolves quartz and hematite phases. Ultimately, this process increases the content of the amorphous gel from 4 to 14%, thereby improving the reactivity of ASW. Overall, the XRD analysis results are in line with the findings of EDAX and SEM analyses. The increased content of the amorphous gel and the particle shape significantly influence the physical and mechanical properties of porous geopolymers.

#### 2.4. Changes in Sodium Stearate during Microwave Exposure

To determine the cause of sample destruction when using sodium stearate, it is necessary to study its interaction with other components. Sodium stearate ( $\text{NaC}_{18}\text{H}_{35}\text{O}_2$ ) is known to be a salt of a carboxylic acid. Carboxylic acids and their salts are characterized by

a decarboxylation reaction (elimination) where a molecule of carbon dioxide is released from the carboxyl or carboxylate group. Examples of such reactions include the Kolbe's reaction, an electrolysis in aqueous solutions of salts, and the Dumas reaction. The Kolbe's reaction occurs only at electrodes, making it an unsuitable option. The Dumas reaction involves fusing salts of carboxylic acids with alkalis (in our case, sodium hydroxide). The reaction of sodium stearate with sodium hydroxide occurs according to Equation (2):



As mentioned earlier, decarboxylation involves the cleavage of the carboxylate group ( $-\text{COONa}$ ), resulting in the formation of heptadecane ( $\text{C}_{17}\text{H}_{36}$ ) and sodium carbonate ( $\text{Na}_2\text{CO}_3$ ), both of which exert negative effects. Heptadecane is an organic compound belonging to the group of alkanes. It possesses low chemical reactivity and can be found in diesel fuel.

It is worth noting that the fusion of sodium stearate with alkali (Equation (2)) occurs only under specific temperatures, which were not found in reference data. Therefore, to identify this temperature and the phase transformations involved, we conducted differential scanning calorimetry using the methodology described in Section 4.3. The DSC curve of the Dumas reaction is presented in Figure 7a. Additionally, to verify the processes occurring during geopolymer synthesis, a DSC analysis of the geopolymer gel of the AS composition was added (Figure 7b).

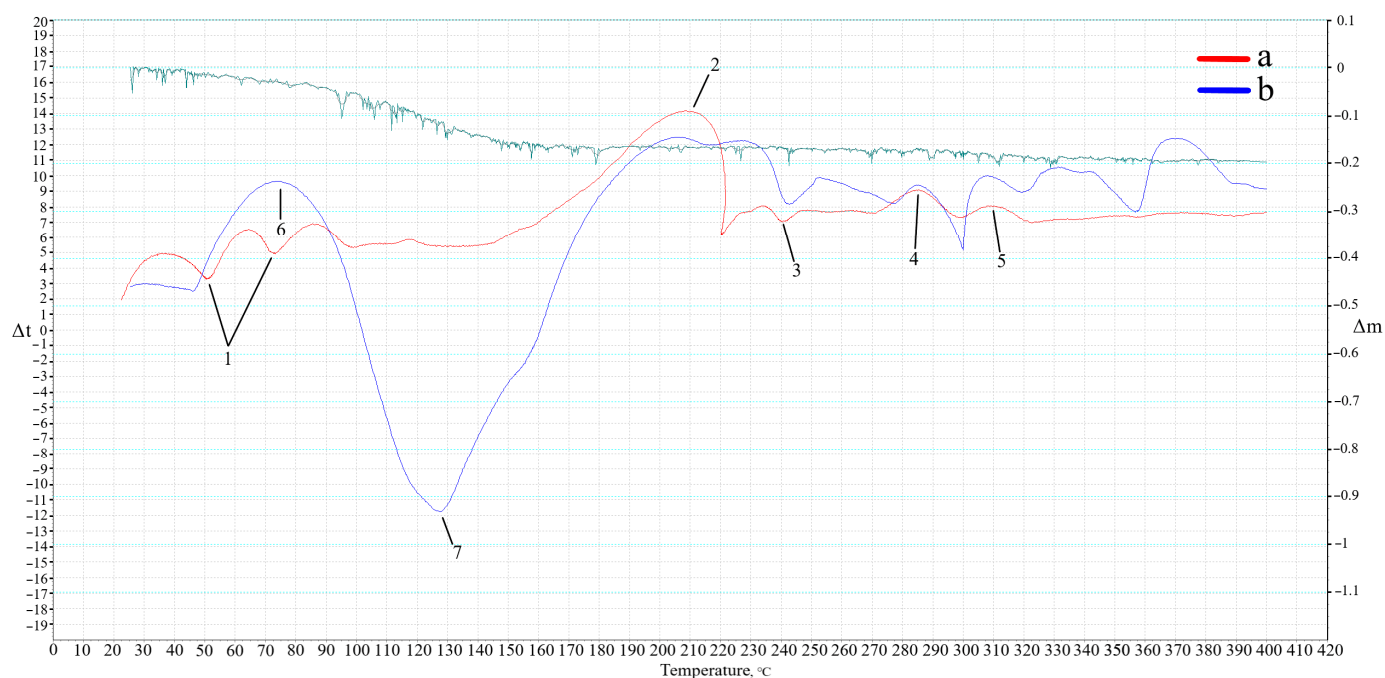


**Figure 7.** DSC curves of the Dumas reaction (a) and geopolymer gel (b).

Analyzing the obtained results of the Dumas reaction, endothermic peaks (1) are observed within the temperature range of 50–100 °C. These peaks are related to the evaporation of physically bound water present in the alkali. The exothermic peak (2) characterizes the reaction temperature according to Equation (2). The initial temperature of the peak is at 145 °C, reaching 221 °C, with an enthalpy of reaction of 45.4 J. The temperature of the peak maximum is at 209 °C, establishing it as the temperature necessary for the reaction to occur. The endothermic peak (3) at 241 °C corresponds to the melting temperature of sodium stearate. Following this, there is an exothermic peak (4) at 287 °C corresponding to the decomposition temperature of sodium stearate within the range of 285–300 °C. The exothermic peak (5) at 305 °C correlates with the boiling temperature of heptadecane.

Examining the DSC results for the geopolymer gel (b), there is partial similarity with the Dumas reaction DSC curve (a), confirming the occurrence of similar processes and phase transformations. However, the intensity of peaks and the sample's mass change during gradual heating differ noticeably. The endothermic peaks (1) experienced the most significant change. The newly formed exothermic peak (6) corresponds to heat release during the interaction between aluminum powder, alkali, and water, resulting in hydrogen release. The mechanism of this reaction was previously described in the research [26]. The endothermic peak (7) corresponds to the partial dissolution of  $\text{SiO}_2$  and  $\text{Al}_2\text{O}_3$  present in ASW, as well as water evaporation from the gel, confirmed by the mass loss curve. The curve of the mass loss of the geopolymer gel at the temperature corresponding to the maximum of the endothermic peak (7) is 14%.

Based on this, a series of tests were conducted to determine the heating temperature of the porous geopolymer under the influence of microwave radiation for 180 s inside molds and 180 s after demolding. Since sample destruction only occurs when using sodium stearate, the tests used the composition A without surfactants. Initially, microwave radiation at 700 W was applied. The obtained results in the form of thermal images are presented in Figure 8. It is worth noting that the images obtained when placing the sample in the microwave oven (0 s) are displayed in a blue spectrum for simplified visualization. This was performed to view the sample at this stage; otherwise, the first image would be entirely black since (according to the scale used, this shade corresponds to temperatures up to 60 °C).

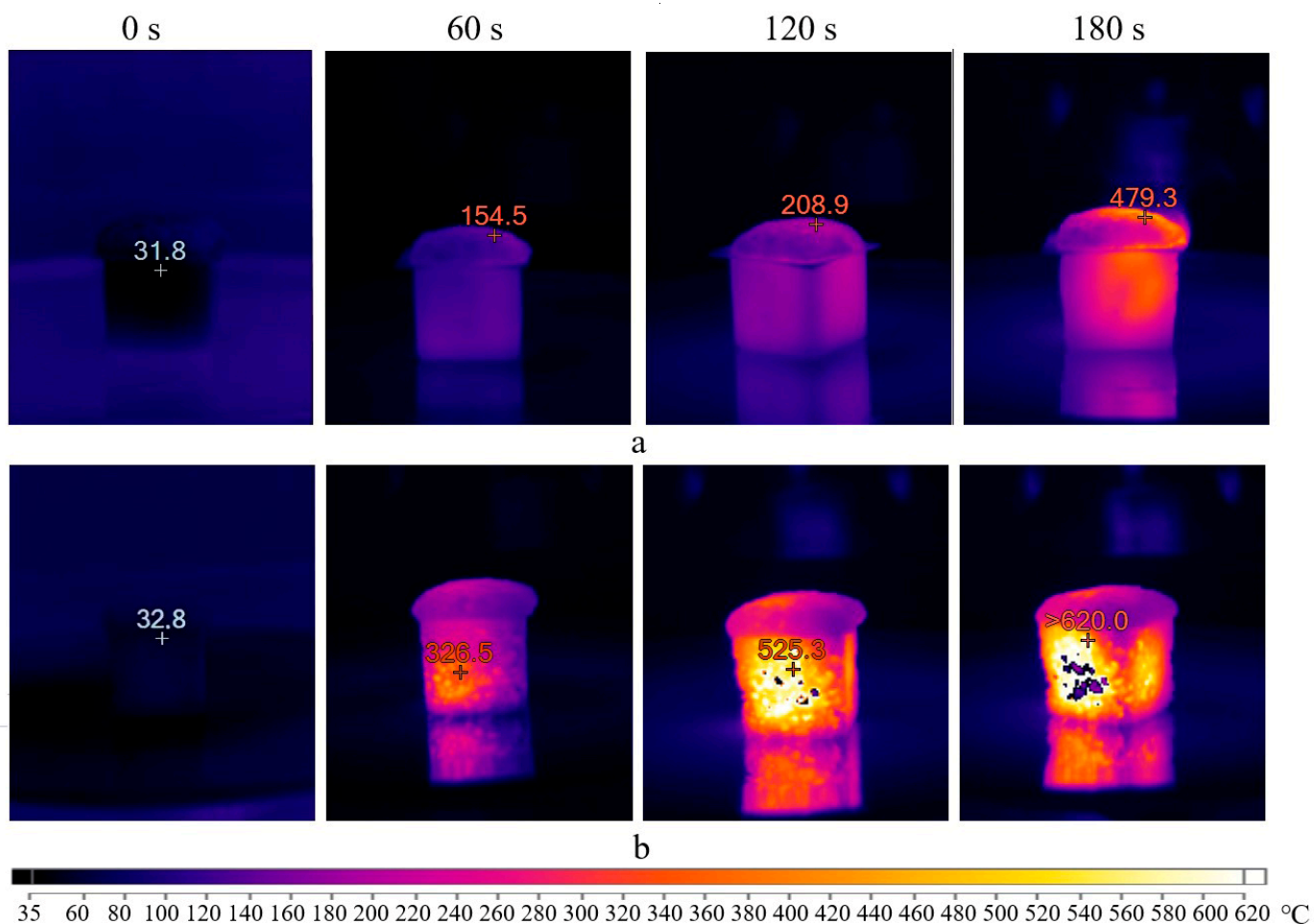


**Figure 8.** Thermal images of the sample exposed to microwave radiation at 700 W inside molds (a) and demolded (b).

The initial temperature of the porous geopolymer was 32 °C. After 60 s, the sample in mold (a) was heated up to 155 °C, corresponding to the start temperature of the Dumas reaction. After 120 s, the sample reached 209 °C, signifying the reaction's completion temperature. At the end of the curing time, the temperature of the sample surface was 480 °C, while the mold temperature exceeded 320 °C. A slight heat flow in the upper right part of the mold was observed after 180 s exposure, attributed to the silicone mold melting.

After cooling, the sample was demolded and placed in the microwave oven. After 60 s, intensive heating of the sample up to 326 °C was observed. This heating intensity was improved by the material's aggregate state and the absence of the silicone mold. It is known that water evaporation and dissolution of silicates and aluminates in the geopolymer mixture occur during the initial curing. Therefore, after 120 s, the samples inside the molds (a) showed less intense heating, compared to demolded ones (b). At the end of the test, the thermal imager recorded temperatures above 620 °C. In the thermal images, these areas fall beyond the device's sensitivity range and appear as empty spots.

The microwave oven used has fixed power settings: maximum—100% (700 W), 50% (350 W), and 10% (70 W), respectively. At 10% microwave power for 5 min, the sample did not heat above 40 °C. Consequently, curing under these conditions would take about 15–20 h. Therefore, the second chosen power level was at 50% of the maximum power, corresponding to 350 W. The results are presented in Figure 9.

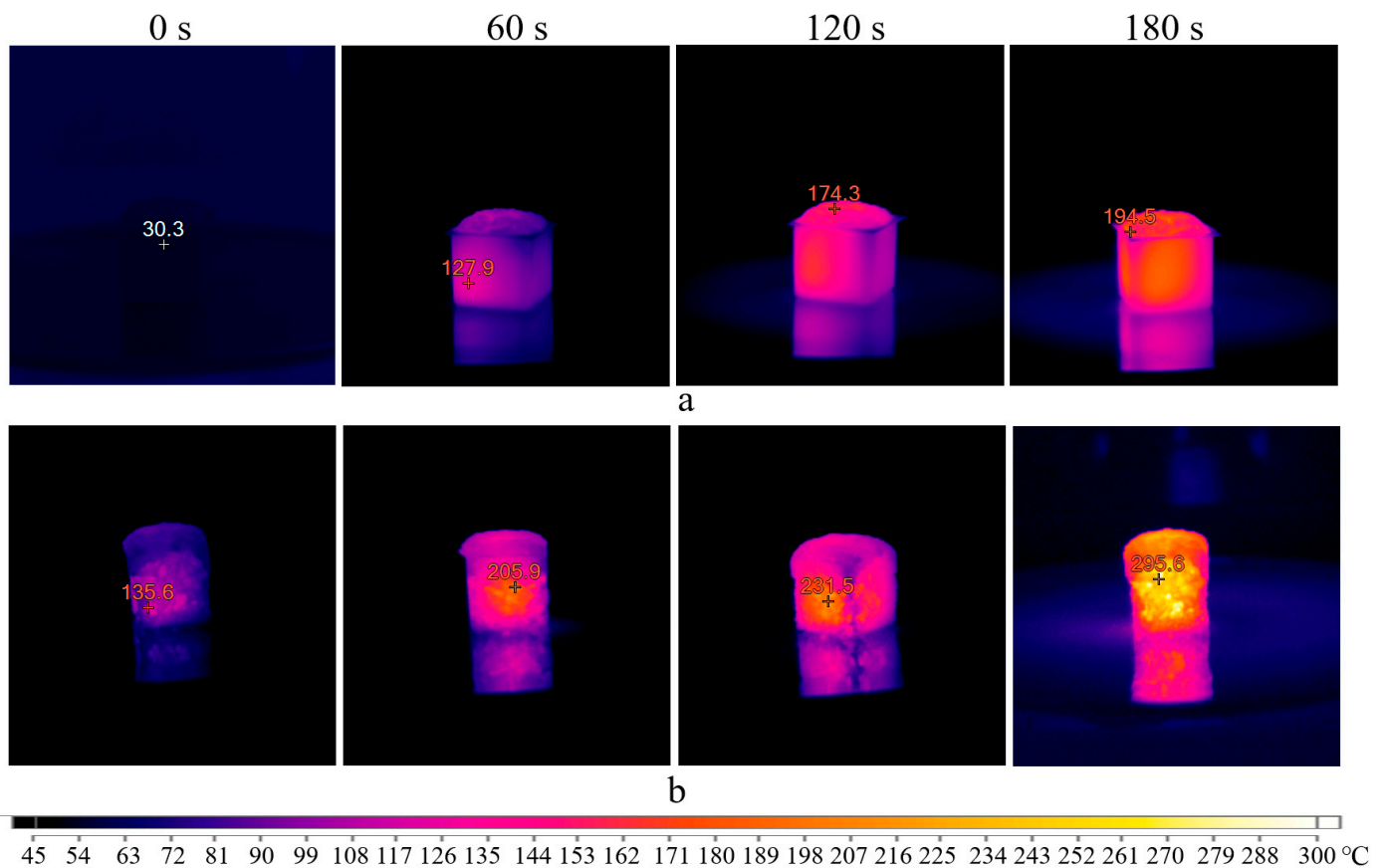


**Figure 9.** Thermal images of the sample exposed to microwave radiation at 350 W inside molds (a) and demolded (b).

The real temperature of the samples would be higher than indicated in the thermal images. This is because it is necessary to stop the microwave oven when capturing these images, which stops heating the sample. As a result, the continuous heating of the sample for 180 s would result in a slightly higher temperature. Therefore, this mode also does not correspond to the synthesis of the AS composition. Interestingly, the thermal images

obtained reveal the degree of sample heating. Initially, the sample heats from the center to the edges, confirming the theory of microwave penetration. Heating the entire volume takes some time. After 180 s, the temperature difference between the central and surface parts of the sample exceeds 100 °C.

To eliminate the possibility of destructive effects of microwave radiation on the structure of sodium stearate, it was decided that the experiment should be repeated using an electric furnace (TK.8.1300.N.1F, Termokeramika, Moscow, Russia). Two modes were used: the first involved placing the geopolymer gel in the furnace preheated up to 300 °C. The second mode involved gradual heating of the sample at a rate of 10 °C/min to a similar temperature. The thermal images are presented in Figure 10.

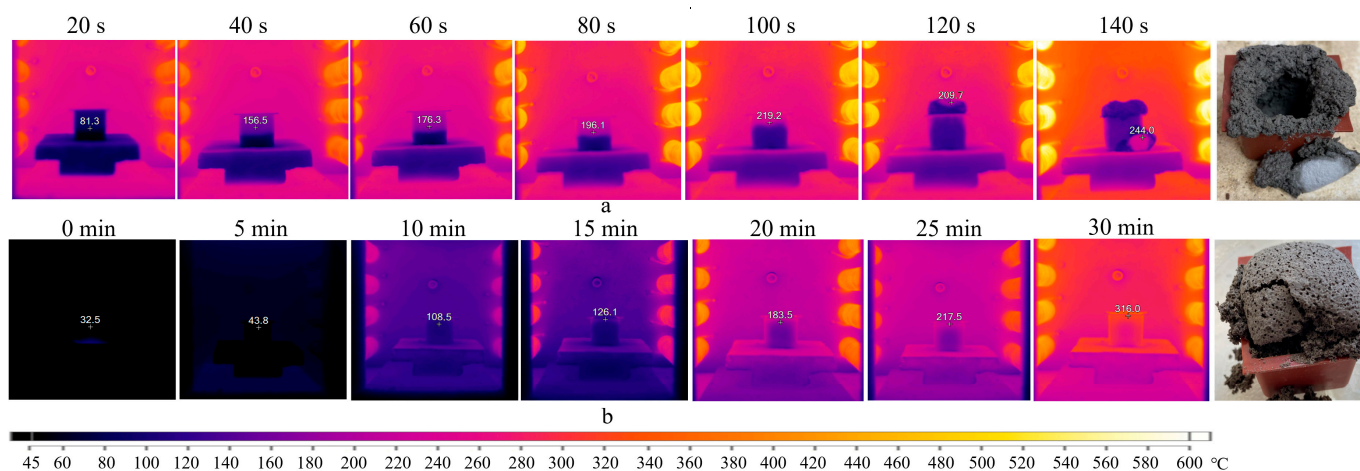


**Figure 10.** Thermal images of the sample exposed to heating in preheated (a) and cold furnace (b).

The series of thermal images (Figure 10a) depicts a similar pattern as observed in the previous experiments. The mold temperature rises to 157 °C in the first 40 s, indicating uneven heating dynamics of the sample. Subsequently, the process stabilizes, and the rate of temperature increase becomes approximately 1 °C/s. At 80 s, the foaming of the geopolymer gel initiates. The temperature of the mold and gel reaches 196 °C and 140 °C, respectively. Between 120–140 s, the sample undergoes destruction in the temperature range of 140–244 °C.

The mode with uniform heating up to 300 °C (Figure 10b) demonstrates nearly similar outcomes. The exception is the appearance of the sample, which maintains its shape. However, the destruction of the geopolymer occurs when demolding it. This indicates that sodium stearate negatively affects the geopolymer structure not only due to intense heating but also because of the Dumas reaction (Equation (2)), resulting in heptadecane formation.

Summarizing the obtained results, it can be concluded that geopolymers of the AS composition react negatively to both sharp and gradual temperature increases during curing, regardless of the heating source. The melting of sodium stearate with sodium hydroxide occurs at temperatures exceeding 130–140 °C. Therefore, temperatures lower than this range are required for a successful synthesis of porous geopolymers with this surfactant. None of the conducted experiments satisfied these conditions.

### 3. Conclusions

The aim of this work was to study the combined influence of curing conditions, surfactants, and waste with different chemical compositions on the foam formation and the physical–chemical properties of porous geopolymers. The findings can be summarized as follows:

- (1) The study of the curing in a drying oven for 6–24 h showed that the difference in physical and mechanical characteristics between 12 and 24 h of curing for the geopolymer gel varied by no more than 5%: the strength increased from 1.02 to

- 1.05 MPa, while the density decreased from 354 to 340 kg/m<sup>3</sup>. Therefore, a 12 h curing period appears more promising from an energy-efficient standpoint.
- (2) Samples containing sodium stearate as a surfactant exhibited the most favorable combination of properties. The following properties were achieved for ASW from different sources: a density of 334 kg/m<sup>3</sup> and a strength of 1.08 MPa for samples based on the ASW from Severodvinsk CHPP-1, and 373 kg/m<sup>3</sup> and 1.17 MPa for samples based on the waste from Novocherkassk SDPP, respectively.
  - (3) The use of microwave radiation allows for achieving the lowest density (291 kg/m<sup>3</sup>) among all samples. The difference between samples' properties cured using microwave radiation for a total of 6 min and cured using a drying oven at 80 °C for 12 h is almost absent. Thus, microwave curing notably reduces the time of the geopolymer gel curing, ultimately streamlining the production of geopolymers.
  - (4) However, microwave irradiation adversely affects the sodium stearate-modified geopolymer gels, leading to complete sample destruction due to the formation of the Dumas reaction. Microwave radiation is found to be incompatible with sodium stearate, suggesting the use of this compound at curing temperatures below 200 °C.
  - (5) Ultimately, the best combination of physical and mechanical properties is exhibited by compositions, utilizing sodium stearate and curing in a drying oven with both types of coal combustion waste. It allows achieving a density of 334 kg/m<sup>3</sup> and a strength of 1.08 MPa for Severodvinsk CHPP-1 and 373 kg/m<sup>3</sup> and 1.17 MPa for Novocherkassk GRES, respectively. Microwave curing stands as a promising method for geopolymer material curing in terms of energy efficiency and time savings. Nonetheless, intensive material heating should be considered when selecting raw materials for its production.

#### 4. Materials and Methods

##### 4.1. Characterization of the Raw Materials

To address the stated task, coal-generated ash and slag waste from the Severodvinsk CHPP-1 (Severodvinsk, Arkhangelsk Oblast, Russia) and Novocherkassk State District Power Plant (SDPP) (Novocherkassk, Rostov Oblast, Russia) were utilized as aluminosilicate raw materials. The chemical and X-ray phase composition of the waste is presented in Figure 11 and Table 5. The true density of the waste from Severodvinsk CHPP-1 is 2034 kg/m<sup>3</sup>, while that from Novocherkassk SDPP is 2321 kg/m<sup>3</sup>.

**Table 5.** Chemical composition of raw materials, wt.%.

Component	SiO <sub>2</sub>	Al <sub>2</sub> O <sub>3</sub>	Fe <sub>2</sub> O <sub>3</sub>	MgO	Na <sub>2</sub> O	K <sub>2</sub> O	CaO	TiO <sub>2</sub>	MnO	P <sub>2</sub> O <sub>5</sub>	SO <sub>3</sub>	LOI
ASW from Severodvinsk CHPP-1	61.6	17.9	6.0	2.7	3.6	2.3	2.1	0.8	0.1	0.2	0.3	2.3
ASW from Novocherkassk SDPP	51.2	18.8	10.3	2.1	0.9	3.0	3.1	0.8	0.1	0.1	0.3	9.2
Waterglass	29.8	0.6	0.1	–	15.3	–	0.2	–	–	–	0.2	53.8
Geopolymer based on ASW from Severodvinsk CHPP-1	49.7	12.7	4.2	1.9	7.7	1.6	1.5	0.6	0.1	0.2	0.3	19.5
Geopolymer based on ASW from Novocherkassk SDPP	42.4	13.3	7.2	1.5	5.8	2.1	2.2	0.6	0.1	0.1	6.5	18.2

The qualitative X-ray phase composition includes crystalline phases such as low quartz (SiO<sub>2</sub>), mullite (3Al<sub>2</sub>O<sub>3</sub> 2SiO<sub>2</sub>), and hematite (Fe<sub>2</sub>O<sub>3</sub>), along with the aluminosilicate glassy phase in the diffraction angles 14–38° (2θ) for the Severodvinsk CHPP-1 waste and 18–30° (2θ) for the Novocherkassk SDPP. The quantitative composition comprises 56.9 ± 0.7% amorphous and 43.1 ± 0.8% crystalline structure (32.4 ± 0.5% low quartz and 10.7 ± 0.3% mullite) for the Severodvinsk CHPP-1 waste. The quantitative composition of the Novocherkassk SDPP waste is reported as 70.2 ± 0.7% amorphous phase and 29.7 ± 0.8% crystalline phase (20.4 ± 0.7% low quartz and 9.3 ± 0.1% hematite).

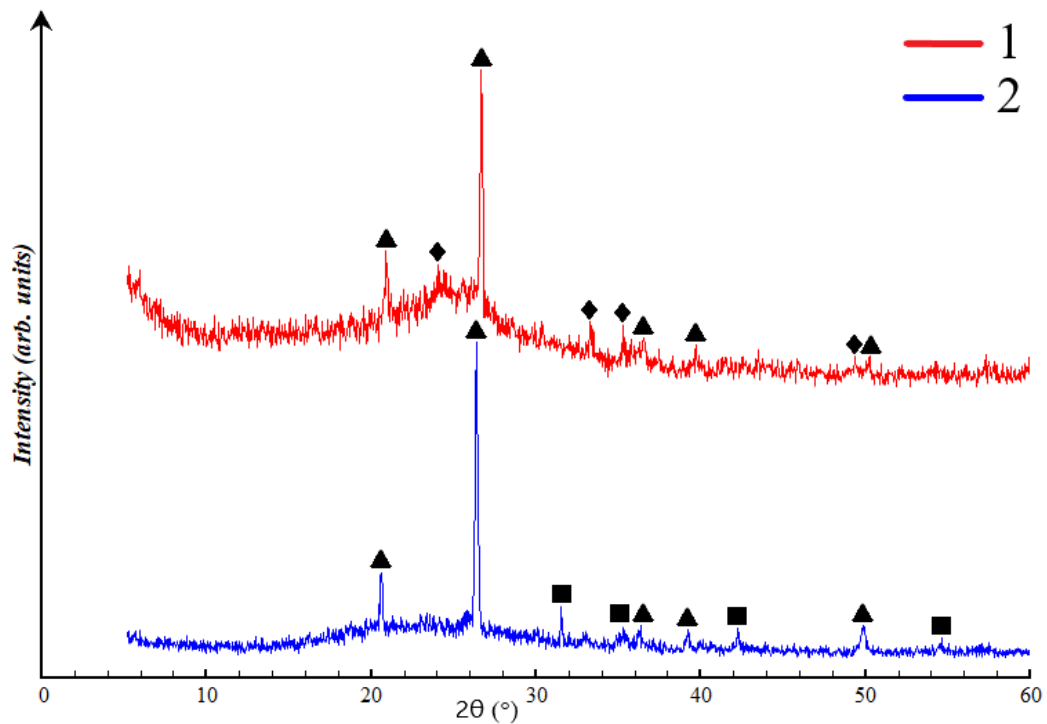


**Figure 11.** X-ray image of ASW: 1—Novocherkassk SDPP, 2—Severodvinsk CHPP-1,  $\Delta$ —low quartz ( $\text{SiO}_2$ ),  $\square$ —mullite ( $3\text{Al}_2\text{O}_3 \cdot 2\text{SiO}_2$ ),  $\diamond$ —hematite ( $\text{Fe}_2\text{O}_3$ ).

Figure 12 shows the particle size distributions of the ASW, determined using a laser particle size analyzer “LASKA-TD” (BioMedSystem, Saint Petersburg, Russia). The particle size for Severodvinsk CHPP-1 is  $D_{50} = 24.94 \mu\text{m}$ ,  $D_{99} = 62.59 \mu\text{m}$ , with a specific surface area of  $54.87 \text{ m}^2/\text{kg}$ . The particle size for Novocherkassk SDPP is  $D_{50} = 40.47 \mu\text{m}$ ,  $D_{99} = 101.10 \mu\text{m}$ , with a specific surface area of  $31.94 \text{ m}^2/\text{kg}$ .

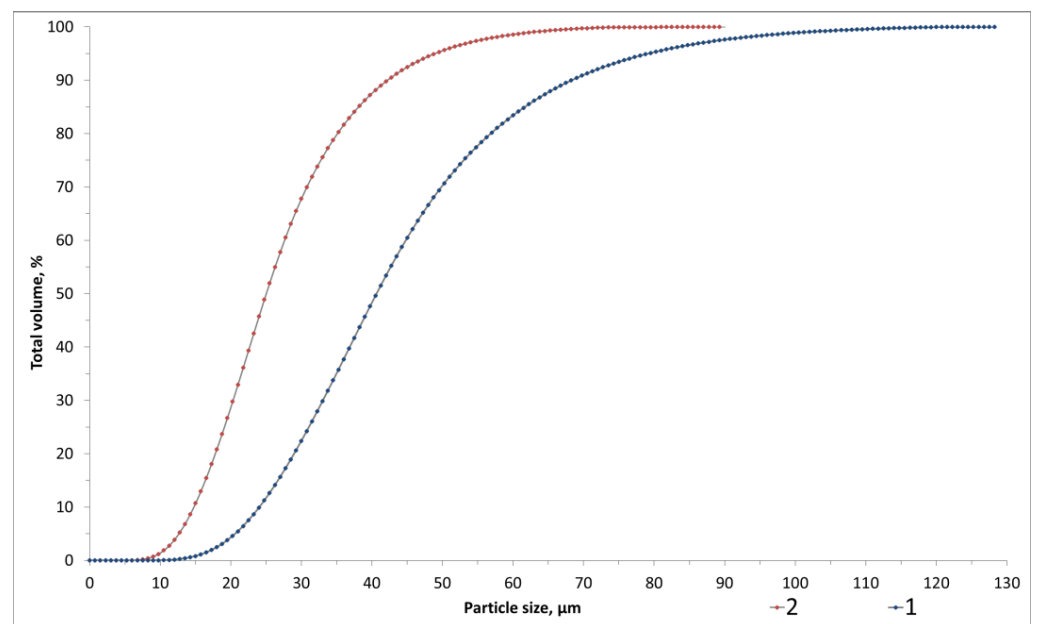


**Figure 12.** Particle size distribution of ASW: 1—Novocherkassk SDPP, 2—Severodvinsk CHPP-1.

For alkaline activation of aluminosilicate materials, a mixture of waterglass (sodium hydrosilicate  $m\text{Na}_2\text{O} \cdot n\text{SiO}_2 \cdot p\text{H}_2\text{O}$ , silicate modulus = 2, water content 53 wt.%, LONTREK,

Moscow, Russia) was used as an activating agent along with a solution of NaOH. As previous studies by the authors have shown [64,65], the optimal molar concentration of NaOH solution ranges from 8 to 12 M, as further increase reduces the compressive strength of foamed geopolymer materials. This conclusion is also supported by research from other authors [66,67]. However, in the study by Xinyu Li [57], the minimum density was achieved at a concentration of 15 mol/L. This indicates that there is no definitive relationship between the concentration of the alkaline activator and the obtained results—each aluminosilicate component requires its specific molar ratio to be determined. Presumably, this effect is achieved due to an increase in the concentration of hydroxide ions that limits their mobility and slows down the formation of coagulation structures [68]. For the preparation of the alkaline solution, a separate container was used, where a pre-weighed portion of granulated NaOH with a purity of 99% (LenReactive, St. Petersburg, Russia) was dissolved in deionized water at a room temperature of  $20 \pm 1$  °C until obtaining a molar concentration of 12 mol/L.

Spherical dispersed aluminum (powder) of ASD-1 grade with a purity of 99% and a specific surface area of  $148 \text{ m}^2/\text{g}$  (GC Metal Energo Holding, Ekaterinburg, Russia) was used as the foaming agent. Olive oil (CHO Company, Sfax, Tunisia) and sodium stearate ( $\text{NaC}_{18}\text{H}_{35}\text{O}_2$ , “Standard”, Moscow, Russia) were employed as surfactants (foam stabilizers).

#### 4.2. Synthesis of Porous Geopolymers

As mentioned earlier, the precursor used was ash and slag waste from the Severodvinsk CHPP-1 and the Novochoerkassk SDPP; the foaming agent—spherical dispersed aluminum, and surfactants—olive oil and sodium stearate. The following notation was used to denote compositions: the coefficient before the composition designates the ASW origin: “N” for Novochoerkassk SDPP and “S” for Severodvinsk CHPP-1; “A” stands for base composition using aluminum powder without surfactants; “AO” includes olive oil, and “AS” includes sodium stearate. Digital designations were used to denote curing modes: 1—drying oven, 2—microwave oven. For instance, the designation “SAO2” describes composition using ASW from Severodvinsk CHPP-1, aluminum powder, and olive oil, cured in a microwave oven. The technology for synthesizing porous geopolymers is presented in Figure 13, and the component compositions of the raw mixture are in Table 6.

**Table 6.** Compositions of studied porous geopolymer mixtures, wt.%.

#	Precursor (ASW)	NaOH (Powder)	Water	Waterglass	Aluminum Powder, over 100	Olive Oil, over 100	Sodium Stearate, over 100
A	70.0	2.5	5.0	22.5	2.0	–	–
AO	70.0	2.5	5.0	22.5	2.0	2.0	–
AS	70.0	2.5	5.0	22.5	2.0	–	2.0

The technology for synthesizing porous geopolymer materials involved the following sequential stages. Initially, the alkali activator was prepared by the method described in Section 4.1. Then, the obtained gel was poured into a pre-weighed aluminosilicate precursor and mixed for 120 s in a mixer (TL-020, DzerzhinskTechnoMash, Dzerzhinsk, Nizhny Novgorod region, Russia) at 300 rpm. After mixing, the geopolymer mixture was supplemented with a foaming agent (aluminum powder) and surfactants (olive oil and sodium stearate), followed by an additional 60 s of mixing under the same conditions.

The resulting mixture was poured into silicone cubic molds with a side length of 30 mm for the following curing. A single-stage, low-temperature solidification was used in a drying oven with forced air convection function (LOIP LF 25/350-VS2, LOIP, Saint Petersburg, Russia) at a temperature of 80 °C for 24 and 12 h, respectively. Additionally, the porous geopolymers were cured using microwave radiation at 700 W and 350 W with a frequency of 2500 MHz in a microwave oven (Midea C4E AM720C4E-S, Midea Group

Co., Ltd., Foshan, China). A two-stage curing mode was employed: 180 s inside molds and 180 s as demolded samples.

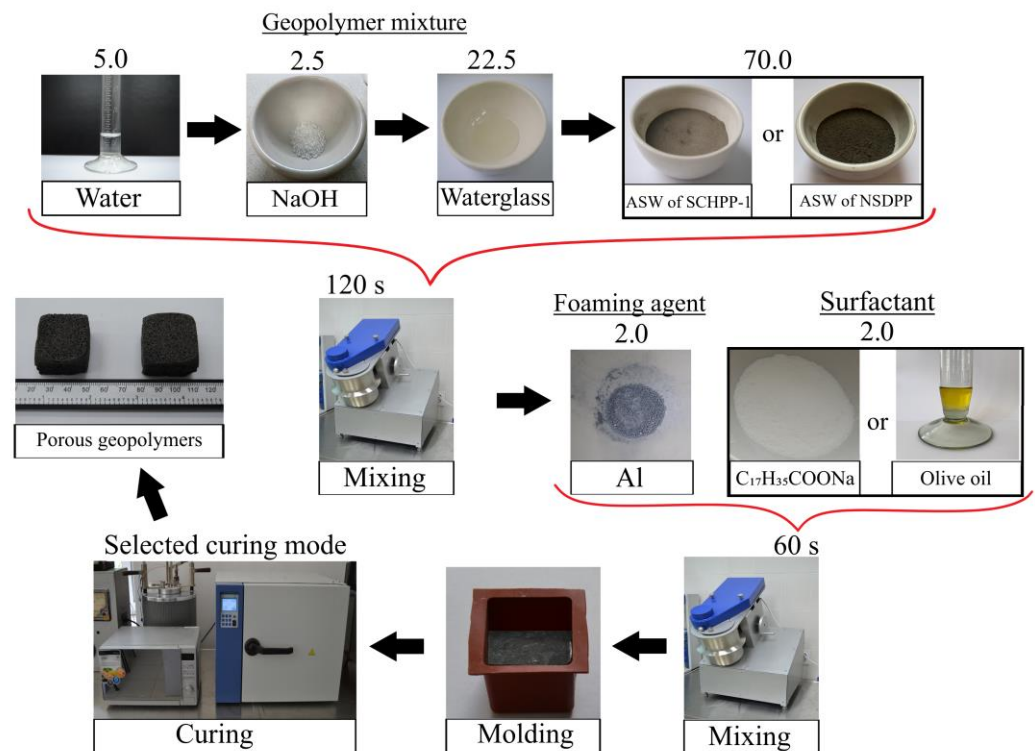


**Figure 13.** Technology of porous geopolymers' synthesis.

#### 4.3. Methods

Qualitative X-ray phase analysis of the synthesized porous geopolymers was conducted using the ARLX'TRA diffractometer (Thermo Fisher Scientific, Waltham, MA, USA) with focused beam reflection via the Bragg–Brentano method. CuK $\alpha$  radiation was employed at 35 kV voltage and with a 30 mA anode current. Diffractograms were recorded in the angular range of 10° to 60° (2 $\theta$ ) with a step size of 0.04°. Data interpretation was carried out using the software package from the ICDD PDF 2 database. Quantitative analysis was performed using the MAUD software (v2.9993 build 532, Materials Analysis Using Diffraction) [69], employing the Rietveld method. The X-ray phase analysis was conducted at the “Nanotechnologies” Collective Use Center of the Platov South-Russian State Polytechnic University (NPI).

Microstructure analysis and EDS (Energy Dispersive Spectroscopy) was conducted using a FEI Quanta 200 scanning electron microscope (FEI Company, Hillsboro, OR, USA). This was coupled with the EDAX Element EDS system (AMETEK, Berwyn, PA, USA). The microanalysis system operated within the following parameters: voltage of 20 kV, magnification (MAG) of 500 $\times$ , Amp Time (ms): 3.84.

The thermal conductivity of the geopolymers was measured using a thermal conductivity meter (ITP-MG4“100/Zond”, SKB StroyPribor, Chelyabinsk, Russia) employing the stationary heat flow method. The temperature of the hot and cold faces was set at 34 °C and 14 °C, respectively. The device measures the sample height, heat flow density, temperature of opposite faces, and based on the acquired data, calculates the effective thermal conductivity  $\lambda$ , W/m·K, according to Equation (3).

$$\lambda = (H \cdot q) / (T_H - T_C), \text{ W/m}\cdot\text{K} \quad (3)$$

where  $\lambda$ —effective thermal conductivity, W/m·K;  $H$ —sample height, cm;  $q$ —density of stationary heat flux passing through the measured sample, W/m<sup>2</sup>;  $T_H$ —temperature of the sample's hot face, K;  $T_C$ —temperature of the sample's cold face, K.

The methodology and equipment necessary for determining the linear dimensions as well as certain physical–mechanical properties (volume, density, porosity, compressive strength) of porous geopolymers were described in the authors' previous research [26,64]. Each recorded test value is the medium of 4 measurements.

The pore size and distribution were automatically assessed using ImageJ freeware [70]. Feret's diameter was used to determine pore sizes, denoting the greatest distance between two points within the pore boundary. High-resolution surface microphotography of samples was conducted using a Stereozoom microscope (SZM-110, The Western Electric & Scientific Works, Haryana, India) equipped with a digital camera (E3ISPM20000KPA IP120000A, Hangzhou ToupTek Photonics Co., Hangzhou, China).

To determine the temperatures of reactions and phase transitions associated with heat release or absorption, differential scanning calorimetry was employed. Analysis was performed using the "Temoskan-2" apparatus (AnalytPribor, St. Petersburg, Russia) with corundum (Al<sub>2</sub>O<sub>3</sub>) used as the reference. Measurements were conducted within a temperature range of 20–400 °C at a heating rate of 10 °C/min. The sample mass used for investigation was 0.5 g.

To determine the surface temperature of the geopolymer, a portable thermal imager (Fluke Ti32, Fluke Corporation, Everett, WA, USA) was used. The temperature was measured by detecting the amount of infrared energy emitted by the sample surface. The device measures temperatures ranging from −20 °C to +600 °C with an accuracy of ±2 °C (but not exceeding 2%). The thermal sensitivity of the device (NETD) at 30 °C is 0.05 °C. Analysis of thermal and visual images was conducted using the built-in software SmartView (v 4.4.363.0, Fluke Thermography, Everett, WA, USA). The emissivity coefficient  $\epsilon$  was set at 0.96, which corresponds to concrete. Throughout the study, including the acquisition of thermal images in both the microwave oven and electric furnace, open-type silicone molds were used. To avoid potential damage to the thermal imager, thermal surface imaging of the geopolymer in the microwave oven was conducted with intermittent operation, as indicated in Figures 8 and 9. Hence, the temperatures recorded in Figures 8 and 9 will be lower than those obtained under continuous microwave exposure for 180 s. To prevent significant heat loss during the cold electric furnace test, the door was closed. The door was opened and imaging was conducted at 5-min intervals. During the acquisition of thermal images in the preheated furnace, the door remained open throughout the experiment. The imaging frequency was limited by the technical capabilities of the thermal imager: specifically, the speed of recording thermal images on the SD memory card (1 frame every 10–12 s) and the automatic calibration of the infrared lens (3–5 s), collectively determining the imaging rate of 1 thermal image per 12–15 s.

**Supplementary Materials:** The following supporting information can be downloaded at: <https://www.mdpi.com/article/10.3390/gels10010019/s1>, Figure S1: Elemental analysis of the surface of porous geopolymers.

**Author Contributions:** E.A.Y. Conceptualization, writing—review and editing, funding acquisition; S.V.T. conceptualization, data curation, writing—original draft preparation; B.M.G. writing—review and editing, supervision; W.L. formal analysis; V.A.S.; methodology; A.V.R. visualization; L.V.K. investigation; A.I.I. visualization. All authors have read and agreed to the published version of the manuscript.

**Funding:** Study of synthesis parameters of geopolymer materials based on ash and slag waste from Severodvinsk CHPP-1 was supported by the Russian Science Foundation (project No. 21-19-00203) "Effective thermo-cured eco-geopolymers for road construction in the Arctic zone of the Russian Federation on the basis of solid fuel combustion wastes from local thermal power plants" (supervisor Yatsenko E.A.). Study of synthesis parameters of geopolymer materials based on ash and slag waste from Novochoerkassk SDPP was supported by the grant of the Ministry of

Science and Higher Education of the Russian Federation No. 075-15-2022-1111 “Carbon-neutral technologies for utilization of large-tonnage fuel and energy wastes with the production of functional geopolymer materials”.

**Institutional Review Board Statement:** Not applicable.

**Informed Consent Statement:** Not applicable.

**Data Availability Statement:** Publicly available datasets were used in this study. This data can be found in the cited references. All data presented in this study are included in the published article.

**Acknowledgments:** The authors want to thank A.N. Yatsenko (the Collective Use Center “Nanotechnologies”, Platov South-Russian State Polytechnic University (NPI)) for the assistance in X-Ray diffraction and SEM analysis.

**Conflicts of Interest:** There are no conflicts of interest in this study.

## References

- Novais, R.M.; Labrincha, J.A. Alkali-Activated Materials as Adsorbents for Water and Wastewater Treatment. In *Alkali-Activated Materials in Environmental Technology Applications*; Woodhead Publishing: Sawston, UK, 2022; pp. 143–166. [\[CrossRef\]](#)
- Chen, S.; Ruan, S.; Zeng, Q.; Liu, Y.; Zhang, M.; Tian, Y.; Yan, D. Pore Structure of Geopolymer Materials and Its Correlations to Engineering Properties: A Review. *Constr. Build. Mater.* **2022**, *328*, 127064. [\[CrossRef\]](#)
- Zhang, X.; Bai, C.; Qiao, Y.; Wang, X.; Jia, D.; Li, H.; Colombo, P. Porous Geopolymer Composites: A Review. *Compos. Part A Appl. Sci. Manuf.* **2021**, *150*, 106629. [\[CrossRef\]](#)
- Ettahiri, Y.; Bouargane, B.; Fritah, K.; Akhsassi, B.; Pérez-Villarejo, L.; Aziz, A.; Bouna, L.; Benlhachemi, A.; Novais, R.M. A State-of-the-Art Review of Recent Advances in Porous Geopolymer: Applications in Adsorption of Inorganic and Organic Contaminants in Water. *Constr. Build. Mater.* **2023**, *395*, 132269. [\[CrossRef\]](#)
- Bai, C.; Colombo, P. Processing, Properties and Applications of Highly Porous Geopolymers: A Review. *Ceram. Int.* **2018**, *44*, 16103–16118. [\[CrossRef\]](#)
- Morsy, M.S.; Rashad, A.M.; Shoukry, H.; Mokhtar, M.M. Potential Use of Limestone in Metakaolin-Based Geopolymer Activated with H<sub>3</sub>PO<sub>4</sub> for Thermal Insulation. *Constr. Build. Mater.* **2019**, *229*, 117088. [\[CrossRef\]](#)
- Rao, P.R.; Momayez, M.; Runge, K.A.; Muralidharan, K. Recent Developments in Thermally Insulating Materials Based on Geopolymers—A Review Article. *Mining Metall. Explor.* **2020**, *37*, 995–1014. [\[CrossRef\]](#)
- Lemougna, P.N.; Wang, K.T.; Tang, Q.; Melo, U.C.; Cui, X.M. Recent Developments on Inorganic Polymers Synthesis and Applications. *Ceram. Int.* **2016**, *42*, 15142–15159. [\[CrossRef\]](#)
- Huang, Y.; Gong, L.; Shi, L.; Cao, W.; Pan, Y.; Cheng, X. Experimental Investigation on the Influencing Factors of Preparing Porous Fly Ash-Based Geopolymer for Insulation Material. *Energy Build.* **2018**, *168*, 9–48. [\[CrossRef\]](#)
- Jaya, N.A.; Yun-Ming, L.; Cheng-Yong, H.; Abdullah, M.M.A.B.; Hussin, K. Correlation between Pore Structure, Compressive Strength and Thermal Conductivity of Porous Metakaolin Geopolymer. *Constr. Build. Mater.* **2020**, *247*, 118641. [\[CrossRef\]](#)
- Huang, Y.; Gong, L.; Pan, Y.; Li, C.; Zhou, T.; Cheng, X. Facile Construction of the Aerogel/Geopolymer Composite with Ultra-Low Thermal Conductivity and High Mechanical Performance. *RSC Adv.* **2018**, *8*, 2350–2356. [\[CrossRef\]](#)
- Cui, Y.; Wang, D.; Zhao, J.; Li, D.; Ng, S.; Rui, Y. Effect of Calcium Stearate Based Foam Stabilizer on Pore Characteristics and Thermal Conductivity of Geopolymer Foam Material. *J. Build. Eng.* **2018**, *20*, 21–29. [\[CrossRef\]](#)
- Tan, T.H.; Mo, K.H.; Ling, T.C.; Lai, S.H. Current Development of Geopolymer as Alternative Adsorbent for Heavy Metal Removal. *Environ. Technol. Innov.* **2020**, *18*, 100684. [\[CrossRef\]](#)
- Tang, J.; Liu, P.; Xue, S.; Li, Y.; Zhao, Y.; Huang, K.; Liu, Z. Optimization of Coal Fly Ash-Based Porous Geopolymer Synthesis and Application for Zinc Removal from Water. *Ceram. Int.* **2023**, *49*, 5828–5833. [\[CrossRef\]](#)
- Łach, M.; Mierzwiński, D.; Korniejewski, K.; Mikula, J. Geopolymer Foam as a Passive Fire Protection. *MATEC Web Conf.* **2018**, *247*, 00031. [\[CrossRef\]](#)
- Sarazin, J.; Davy, C.A.; Bourbigot, S.; Tricot, G.; Hosdez, J.; Lambertin, D.; Fontaine, G. Flame Resistance of Geopolymer Foam Coatings for the Fire Protection of Steel. *Compos. Part B Eng.* **2021**, *222*, 109045. [\[CrossRef\]](#)
- Sharma, S.; Medpelli, D.; Chen, S.; Seo, D.K. Calcium-Modified Hierarchically Porous Aluminosilicate Geopolymer as a Highly Efficient Regenerable Catalyst for Biodiesel Production. *RSC Adv.* **2015**, *5*, 65454–65461. [\[CrossRef\]](#)
- Innocentini, M.D.M.; Botti, R.F.; Bassi, P.M.; Paschoalato, C.F.P.R.; Flumignan, D.L.; Franchin, G.; Colombo, P. Lattice-Shaped Geopolymer Catalyst for Biodiesel Synthesis Fabricated by Additive Manufacturing. *Ceram. Int.* **2019**, *45*, 1443–1446. [\[CrossRef\]](#)
- Zhang, Z.; Wang, K.; Mo, B.; Li, X.; Cui, X. Preparation and Characterization of a Reflective and Heat Insulative Coating Based on Geopolymers. *Energy Build.* **2015**, *87*, 220–225. [\[CrossRef\]](#)
- Gao, H.; Liu, H.; Liao, L.; Mei, L.; Zhang, F.; Zhang, L.; Li, S.; Lv, G. A Bifunctional Hierarchical Porous Kaolinite Geopolymer with Good Performance in Thermal and Sound Insulation. *Constr. Build. Mater.* **2020**, *251*, 118888. [\[CrossRef\]](#)
- Reeb, C.; Pierlot, C.; Davy, C.; Lambertin, D. Incorporation of Organic Liquids into Geopolymer Materials—A Review of Processing, Properties and Applications. *Ceram. Int.* **2021**, *47*, 7369–7385. [\[CrossRef\]](#)

22. Beleuk à Moungam, L.M.; Lemougna, P.N.; Kaze, R.C.; Mohamed, H.; Deutou Nemaleu, J.G.; Billong, N.; Kamseu, E.; Mvondo-Ze, A.D.; Tonle Kenfack, I. Synthesis of Volcanic Ash-based Porous Inorganic Polymers Using Biomass as Pore Inducing Agent: Phase Evolution and Descriptive Microstructure. *Silicon* **2022**, *14*, 2595–2608. [[CrossRef](#)]
23. Beleuk à Moungam, L.M.; Tchieda, K.V.; Mohamed, H.; Pecheu, N.C.; Kaze, R.C.; Kamseu, E.; Mvondo-Ze, A.D.; Tonle, I.K. Efficiency of Volcanic Ash-Based Porous Geopolymers for the Removal of Pb<sup>2+</sup>, Cd<sup>2+</sup> and Hg<sup>2+</sup> from Aqueous Solution. *Clean. Mater.* **2022**, *5*, 100106. [[CrossRef](#)]
24. Zivica, V.; Palou, M.T.; Bágel, T.I.L. High Strength Metahalloysite Based Geopolymer. *Compos. Part B Eng.* **2014**, *57*, 155–165. [[CrossRef](#)]
25. Bai, C.; Franchin, G.; Elsayed, H.; Conte, A.; Colombo, P. High Strength Metakaolin-Based Geopolymer Foams with Variable Macroporous Structure. *J. Eur. Ceram. Soc.* **2016**, *36*, 4243–4249. [[CrossRef](#)]
26. Yatsenko, E.A.; Goltsman, B.M.; Trofimov, S.V.; Novikov, Y.V.; Smolij, V.A.; Ryabova, A.V.; Klimova, L.V. Influence of Various Coal Energy Wastes and Foaming Agents on Foamed Geopolymer Materials' Synthesis. *Materials* **2023**, *16*, 264. [[CrossRef](#)] [[PubMed](#)]
27. Zhang, P.; Gao, Z.; Wang, J.; Guo, J.; Hu, S.; Ling, Y. Properties of Fresh and Hardened Fly Ash/Slag Based Geopolymer Concrete: A Review. *J. Clean. Prod.* **2020**, *270*, 122389. [[CrossRef](#)]
28. Almalkawi, A.T.; Balchandra, A.; Soroushian, P. Potential of Using Industrial Wastes for Production of Geopolymer Binder as Green Construction Materials. *Constr. Build. Mater.* **2019**, *220*, 516–524. [[CrossRef](#)]
29. Zhu, Z.; Zhang, C.; Liu, R.; Li, S.; Wang, M. Sunflower Straw Ash as an Alternative Activator in Alkali-Activated Grouts: A New 100% Waste-Based Material. *Ceram. Int.* **2023**, *49*, 32308–32312. [[CrossRef](#)]
30. Çelik, A.İ.; Tunç, U.; Bahrami, A.; Karalar, M.; Othuman Mydin, M.A.; Alomayri, T.; Özkılıç, Y.O. Use of Waste Glass Powder toward More Sustainable Geopolymer Concrete. *J. Mater. Res. Technol.* **2023**, *24*, 8533–8546. [[CrossRef](#)]
31. Lau, C.K.; Rowles, M.R.; Parnham, G.N.; Htut, T.; Ng, T.S. Investigation of Geopolymers Containing Fly Ash and Ground-Granulated Blast-Furnace Slag Blended by Amorphous Ratios. *Constr. Build. Mater.* **2019**, *222*, 731–737. [[CrossRef](#)]
32. Zimar, Z.; Robert, D.; Zhou, A.; Giustozzi, F.; Setunge, S.; Kodikara, J. Application of Coal Fly Ash in Pavement Subgrade Stabilisation: A Review. *J. Environ. Manag.* **2022**, *312*, 114926. [[CrossRef](#)] [[PubMed](#)]
33. Onyelowe, K.C.; Kontoni, D.P.N.; Ebid, A.M.; Dabbaghi, F.; Soleymani, A.; Jahangir, H.; Nehdi, M.L. Multi-Objective Optimization of Sustainable Concrete Containing Fly Ash Based on Environmental and Mechanical Considerations. *Buildings* **2022**, *12*, 948. [[CrossRef](#)]
34. El Alouani, M.; Aouan, B.; Rachdi, Y.; Alehyen, S.; El Herradi, E.H.; Saufi, H.; Mabrouki, J.; Barka, N. Porous Geopolymers as Innovative Adsorbents for the Removal of Organic and Inorganic Hazardous Substances: A Mini-Review. *Int. J. Environ. Anal. Chem.* **2022**. [[CrossRef](#)]
35. Kočí, V.; Černý, R. Directly Foamed Geopolymers: A Review of Recent Studies. *Cem. Concr. Compos.* **2022**, *130*, 104530. [[CrossRef](#)]
36. Matalkah, F.; Ababneh, A.; Aqel, R. Synthesis of Calcined Kaolin-Based Geopolymer Foam: Assessment of Mechanical Properties, Thermal Insulation, and Elevated Temperature Stability. *Ceram. Int.* **2023**, *49*, 9967–9977. [[CrossRef](#)]
37. Yan, S.; Zhang, F.; Liu, J.; Ren, B.; He, P.; Jia, D.; Yang, J. Green Synthesis of High Porosity Waste Gangue Microsphere/Geopolymer Composite Foams via Hydrogen Peroxide Modification. *J. Clean. Prod.* **2019**, *227*, 483–494. [[CrossRef](#)]
38. Kioupis, D.; Zisimopoulou, A.; Tsivilis, S.; Kakali, G. Development of Porous Geopolymers Foamed by Aluminum and Zinc Powders. *Ceram. Int.* **2021**, *47*, 26280–26292. [[CrossRef](#)]
39. Kaczmarek, K.; Pławecka, K.; Kozub, B.; Bazan, P.; Łach, M. Preliminary Investigation of Geopolymer Foams as Coating Materials. *Appl. Sci.* **2022**, *12*, 11205. [[CrossRef](#)]
40. Liang, B.; Zhang, M.; Li, H.; Zhao, M.; Xu, P.; Deng, L. Preparation of Ceramic Foams from Ceramic Tile Polishing Waste and Fly Ash without Added Foaming Agent. *Ceram. Int.* **2021**, *47*, 23338–23349. [[CrossRef](#)]
41. Liu, X.; Hu, C.; Chu, L. Microstructure, Compressive Strength and Sound Insulation Property of Fly Ash-Based Geopolymeric Foams with Silica Fume as Foaming Agent. *Materials* **2020**, *13*, 3215. [[CrossRef](#)]
42. Abdollahnejad, Z.; Pacheco-Torgal, F.; Félix, T.; Tahri, W.; Barroso Aguiar, J. Mix Design, Properties and Cost Analysis of Fly Ash-Based Geopolymer Foam. *Constr. Build. Mater.* **2015**, *80*, 18–30. [[CrossRef](#)]
43. Novais, R.M.; Pullar, R.C.; Labrincha, J.A. Geopolymer Foams: An Overview of Recent Advancements. *Prog. Mater. Sci.* **2020**, *109*, 100621. [[CrossRef](#)]
44. Yu, Q.; Li, X.; Wang, Z.; Xue, J. Characterization and Performance Evaluation of Metakaolin-Based Geopolymer Foams Obtained by Adding Palm Olein as the Foam Stabilizer. *Materials* **2022**, *15*, 3570. [[CrossRef](#)] [[PubMed](#)]
45. Wang, Z.; Lu, D. Study on the Effect of Emulsifiers on the Pore Structures of Geopolymer Prepared by Emulsion Templating. *Mater. Res. Express* **2020**, *7*, 055508. [[CrossRef](#)]
46. Dong, C.; Shao, N.; Yan, F.; Ji, R.; Wei, X.; Zhang, Z. A Novel Integration Strategy for the Foaming and Hydrophobization of Geopolymer Foams. *Cem. Concr. Res.* **2022**, *160*, 106919. [[CrossRef](#)]
47. Xu, F.; Gu, G.; Zhang, W.; Wang, H.; Huang, X.; Zhu, J. Pore Structure Analysis and Properties Evaluations of Fly Ash-Based Geopolymer Foams by Chemical Foaming Method. *Ceram. Int.* **2018**, *44*, 19989–19997. [[CrossRef](#)]
48. Li, X.; Bai, C.; Qiao, Y.; Wang, X.; Yang, K.; Colombo, P. Preparation, Properties and Applications of Fly Ash-Based Porous Geopolymers: A Review. *J. Clean. Prod.* **2022**, *359*, 132043. [[CrossRef](#)]
49. Raza, A.; Hechmi El Ouni, M.; Azab, M.; Ali, K.; Haider, H.; Rashedi, A. A Scientometric Review on Mechanical and Durability Performance of Geopolymer Paste: Effect of Various Raw Materials. *Constr. Build. Mater.* **2022**, *345*, 128297. [[CrossRef](#)]

50. Rovnanik, P. Effect of Curing Temperature on the Development of Hard Structure of Metakaolin-Based Geopolymer. *Constr. Build. Mater.* **2010**, *24*, 1176–1183. [[CrossRef](#)]
51. Bai, C.; Colombo, P. High-Porosity Geopolymer Membrane Supports by Peroxide Route with the Addition of Egg White as Surfactant. *Ceram. Int.* **2017**, *43*, 2267–2273. [[CrossRef](#)]
52. Alghamdi, H.; Dakhane, A.; Alum, A.; Abbaszadegan, M.; Mobasher, B.; Neithalath, N. Synthesis and Characterization of Economical, Multi-Functional Porous Ceramics Based on Abundant Aluminosilicates. *Mater. Des.* **2018**, *152*, 10–21. [[CrossRef](#)]
53. Onutai, S.; Jiemsirilars, S.; Thavorniti, P.; Kobayashi, T. Fast Microwave Syntheses of Fly Ash Based Porous Geopolymers in the Presence of High Alkali Concentration. *Ceram. Int.* **2016**, *42*, 9866–9874. [[CrossRef](#)]
54. Li, X.; Zheng, J.; Shao, J.; Loutou, M.; Bai, C.; Qiao, Y.; Miao, Y.; Wang, X.; Zheng, T.; Colombo, P. Evaluation of Porosity, Mechanical and Thermal Properties of Self-Ignition Coal Gangue-Based Foams via Fast Microwave Foaming. *J. Build. Eng.* **2023**, *68*, 106062. [[CrossRef](#)]
55. Nadeem, M.; Ul Haq, E.; Ahmed, F.; Asif Rafiq, M.; Hameed Awan, G.; Zain-ul-Abdein, M. Effect of Microwave Curing on the Construction Properties of Natural Soil Based Geopolymer Foam. *Constr. Build. Mater.* **2020**, *230*, 117074. [[CrossRef](#)]
56. Ul Haq, E.; Kunjalukal Padmanabhan, S.; Licciulli, A. Microwave Synthesis of Thermal Insulating Foams from Coal Derived Bottom Ash. *Fuel Process. Technol.* **2015**, *130*, 263–267. [[CrossRef](#)]
57. Li, X.; Liu, L.; Bai, C.; Yang, K.; Zheng, T.; Lu, S.; Li, H.; Qiao, Y.; Colombo, P. Porous Alkali-Activated Material from Hypergolic Coal Gangue by Microwave Foaming for Methylene Blue Removal. *J. Am. Ceram. Soc.* **2023**, *106*, 1473–1489. [[CrossRef](#)]
58. Nguyen, T.T.; Goodier, C.I.; Austin, S.A. Factors Affecting the Slump and Strength Development of Geopolymer Concrete. *Constr. Build. Mater.* **2020**, *261*, 119945. [[CrossRef](#)]
59. Bai, B.; Bai, F.; Nie, Q.; Jia, X. A High-Strength Red Mud–Fly Ash Geopolymer and the Implications of Curing Temperature. *Powder Technol.* **2023**, *416*, 118242. [[CrossRef](#)]
60. Leiva, C.; Luna-Galiano, Y.; Arenas, C.; Alonso-Fariñas, B.; Fernández-Pereira, C. A Porous Geopolymer Based on Aluminum-Waste with Acoustic Properties. *Waste Manag.* **2019**, *95*, 504–512. [[CrossRef](#)]
61. Shao, J.; Bai, C.; Li, X.; Yang, K.; Zheng, T.; Qiao, Y.; Zhang, L.; Li, H.; Colombo, P. Open-Cell Mullite Ceramic Foams Derived from Porous Geopolymer Precursors with Tailored Porosity. *J. Adv. Ceram.* **2023**, *12*, 279–295. [[CrossRef](#)]
62. Ji, Z.; Li, M.; Su, L.; Pei, Y. Porosity, Mechanical Strength and Structure of Waste-Based Geopolymer Foams by Different Stabilizing Agents. *Constr. Build. Mater.* **2020**, *258*, 119555. [[CrossRef](#)]
63. Hosseini, S.; Brake, N.A.; Nikookar, M.; Günaydın-Şen, Ö.; Snyder, H.A. Mechanochemically Activated Bottom Ash-Fly Ash Geopolymer. *Cem. Concr. Compos.* **2021**, *118*, 103976. [[CrossRef](#)]
64. Yatsenko, E.A.; Goltsman, B.M.; Trofimov, S.V.; Kurdashov, V.M.; Novikov, Y.V.; Smolij, V.A.; Ryabova, A.V.; Klimova, L. V Improving the Properties of Porous Geopolymers Based on TPP Ash and Slag Waste by Adjusting Their Chemical Composition. *Materials* **2022**, *15*, 2587. [[CrossRef](#)] [[PubMed](#)]
65. Yatsenko, E.A.; Goltsman, B.M.; Trofimov, S.V.; Lazorenko, G.I. Processing of Ash and Slag Waste from Coal Fuel Combustion at CHPPs in the Arctic Zone of Russia with Obtaining Porous Geopolymer Materials. *Therm. Eng.* **2022**, *69*, 615–623. [[CrossRef](#)]
66. Nuruddin, M.F.; Demie, S.; Ahmed, M.F.; Shafiq, N. Effect of Superplasticizer and NaOH Molarity on Workability, Compressive Strength and Microstructure Properties of Self-Compacting Geopolymer Concrete. *World Acad. Sci. Eng. Technol.* **2011**, *51*, 187–194.
67. Chithambar Ganesh, A.; Muthukannan, M.; Aakassh, S.; Prasad; Subramanaian, B. Energy Efficient Production of Geopolymer Bricks Using Industrial Waste. In *Proceedings of the IOP Conference Series: Materials Science and Engineering*; IOP Publishing: Bristol, UK, 2020; Volume 872, p. 012154. [[CrossRef](#)]
68. Hashim, M.F.A.; Faris, M.A.; Mydin, M.A.O.; Ghazali, C.M.R.; Daud, Y.M.; Abdullah, M.M.A.B.; Zainal, F.F.; Mohd Tahir, M.F.; Yong, H.C.; Khorami, M. Interaction of Geopolymer Filler and Alkali Molarity Concentration towards the Fire Properties of Glass-Reinforced Epoxy Composites Fabricated Using Filament Winding Technique. *Materials* **2022**, *15*, 6495. [[CrossRef](#)]
69. Luca Lutterotti MAUD—Materials Analysis Using Diffraction. Available online: <https://luttero.github.io/maud/> (accessed on 21 August 2023).
70. National Institutes of Health Image J. Available online: <https://imagej.net/ij/index.html> (accessed on 21 August 2023).

**Disclaimer/Publisher’s Note:** The statements, opinions and data contained in all publications are solely those of the individual author(s) and contributor(s) and not of MDPI and/or the editor(s). MDPI and/or the editor(s) disclaim responsibility for any injury to people or property resulting from any ideas, methods, instructions or products referred to in the content.